Journal of Hydrology

Sequential and Coupled Inversion of Horizontal Borehole Ground Penetrating Radar Data to Estimate Soil Hydraulic Properties at the Field Scale

--Manuscript Draft--

Manuscript Number:	HYDROL38361R1
Article Type:	Research paper
Keywords:	Ground penetrating radar; hydrogeophysics; coupled inversion.
Corresponding Author:	Yi Yu IBG-3 juelich, GERMANY
First Author:	Yi Yu
Order of Authors:	Yi Yu
	Lutz Weihermüller
	Anja Klotzsche
	Lena Lärm
	Harry Vereecken
	Johan A Huisman
Abstract:	Horizontal borehole ground penetrating radar (GPR) measurements can provide valuable information on soil water content (SWC) dynamics in the vadose zone, and hence show potential to estimate soil hydraulic properties. In this study, the performance of both sequential and coupled inversion workflows to obtain soil hydraulic properties from time-lapse horizontal borehole GPR data obtained during an infiltration experiment were compared using a synthetic modelling study and the analysis of actual field data. The sequential inversion using the vadose zone flow model HYDRUS-1D directly relied on SWC profiles determined from the travel time of GPR direct waves using the straight-wave approximation. The synthetic modelling study showed that sequential inversion did not provide accurate estimates of the soil hydraulic parameters due to interpretation errors in the estimated SWC near the infiltration front and the ground surface. In contrast, the coupled inversion approach, which combined HYDRUS-1D with a forward model of GPR wave propagation (gprMax3D) and GPR travel time information, provided accurate estimates of the hydraulic properties in the synthetic modelling study. The application of the coupled inversion approach to measured borehole GPR data also resulted in plausible estimates of the soil hydraulic parameters. It was concluded that coupled inversion should be preferred over sequential inversion of time-lapse horizontal borehole GPR data in the presence of strong SWC gradients that occur during infiltration events.
Suggested Reviewers:	Majken Caroline Looms Associate Professor mcl@ign.ku.dk
	Adam Mangel adam.mangel@pnnl.gov
	Matteo Rossi matteo.rossi@tg.lth.se
	Colby Steelman cmsteelman@uwaterloo.ca
	Niels Claes ncl@geo.au.dk
	Rita Deiana rita.deiana@unipd.it
	Stephen Moysey

	moyseys18@ecu.edu
	Erasmus Oware erasmuso@buffalo.edu
Response to Reviewers:	

Abstract

Horizontal borehole ground penetrating radar (GPR) measurements can provide valuable information on soil water content (SWC) dynamics in the vadose zone, and hence show potential to estimate soil hydraulic properties. In this study, the performance of both sequential and coupled inversion workflows to obtain soil hydraulic properties from time-lapse horizontal borehole GPR data obtained during an infiltration experiment were compared using a synthetic modelling study and the analysis of actual field data. The sequential inversion using the vadose zone flow model HYDRUS-1D directly relied on SWC profiles determined from the travel time of GPR direct waves using the straight-wave approximation. The synthetic modelling study showed that sequential inversion did not provide accurate estimates of the soil hydraulic parameters due to interpretation errors in the estimated SWC near the infiltration front and the ground surface. In contrast, the coupled inversion approach, which combined HYDRUS-1D with a forward model of GPR wave propagation (gprMax3D) and GPR travel time information, provided accurate estimates of the hydraulic properties in the synthetic modelling study. The application of the coupled inversion approach to measured borehole GPR data also resulted in plausible estimates of the soil hydraulic parameters. It was concluded that coupled inversion should be preferred over sequential inversion of time-lapse horizontal borehole GPR data in the presence of strong SWC gradients that occur during infiltration events.

Key Words: Ground penetrating radar, hydrogeophysics, coupled inversion.

*Highlights (3 to 5 bullet points (maximum 85 characters including spaces per bullet point)

- Sequential inversion of ground penetrating radar data cannot provide accurate hydraulic parameter estimates if strong vertical gradients in soil water content are present due to infiltration.
- Coupled inversion of ground penetrating radar data is able to provide accurate estimates of the hydraulic parameters.
- Hydraulic parameters estimated using coupled inversion of experimental ground penetrating radar data were consistent with water retention and relative hydraulic conductivity functions from independent time domain reflectometry measurements.

Sequential and Coupled Inversion of Horizontal Borehole Ground Penetrating Radar Data to Estimate Soil Hydraulic Properties at the Field Scale

Yi Yu[1,2], Lutz Weihermüller[1], Anja Klotzsche[1,2], Lena Lärm[1], Harry Vereecken[1] and Johan Alexander Huisman[1]

[1]Agrosphere (IBG-3), Institute of Bio- and Geosciences, Forschungszentrum Jülich GmbH, 52425 Jülich, Germany

[2]HPSC TerrSys, Centre for High-Performance Scientific Computing in Terrestrial Systems, Geoverbund ABC/J, Jülich, Germany

Corresponding author: Yi Yu, email: y.yu@fz-juelich.de

1. Introduction

Obtaining accurate hydraulic parameters of the vadose zone is important in a wide range of applications, including modelling of water flow and contaminant transport (e.g., Wagner, 1992; Vereecken; et al., 2007), managing water and soil resources (e.g., Blanco-Canqui and Lai, 2007; Hartmann et al., 2014), and evaluating climate change effects on forests (e.g., Martínez-Vilalta et al., 2002; McDowell and Allen, 2015). Hydraulic parameters can be determined by different laboratory methods (e.g., Neuzil et al., 1981), but this typically leads to hydraulic property estimates that are not representative of field conditions (Kool et al., 1987). Therefore, estimation of hydraulic properties at the field scale is preferred if characterization at this scale is intended (Klute and Dirksen, 1986).

Field-scale estimation of hydraulic properties is commonly based on measurements made with point-scale sensors, such as the neutron probe (Chanasyk and Naeth, 1996) and time domain reflectometry (TDR) (Robinson et al., 2008). Such methods allow the accurate determination of soil water content (SWC) dynamics, and therefore have been widely used for parameterizing hydrological models (e.g., Abbaspour et al., 2000; Katul et al., 1993; Kumar et al., 2010; Malicki et al., 1992; Nandagiri and Prasad, 1996; Steenpass et al., 2010; Wollschläger et al., 2009). In some studies, SWC measurements were combined with matric potential measurements obtained by tensiometers (e.g., Zhang et al., 2003) in order to better constrain the hydraulic parameter estimation (Vereecken et al., 2008). A major disadvantage of using point sensor information to estimate soil hydraulic properties is the relatively small sensing volume and the resulting limited representativeness for the field-scale soil states.

In the last decades, many studies reported the potential of using geophysical techniques, such as electromagnetic induction (EMI) (e.g., Brosten et al., 2011; Moghadas et al., 2017), electrical resistivity tomography (ERT) (e.g., Brunet et al., 2010; Huisman et al., 2010; Manoli et al., 2015; Mboh et al., 2012; Pollock and Cirpka, 2010) and ground penetrating radar (GPR) (e.g., Hubbard and Rubin, 2000; Looms et al., 2008a; Rossi et al., 2015), to obtain accurate field-scale estimates of SWC and soil hydraulic properties. GPR uses the travel time and attenuation of high-frequency electromagnetic waves travelling through the ground to obtain the dielectric permittivity (ε) and electric conductivity (σ) of the subsurface (e.g., Holliger et al., 2001; Slob et al., 2010). Due to the direct relationship between ε and SWC (Topp et al., 1980), GPR is the one of the most promising geophysical methods for SWC estimation (e.g., Huisman et al., 2003; Klotzsche et al., 2018). GPR can rapidly provide surveys for larger scales of interest (1 ~ 1000 m profiles) (e.g., Mahmoudzadeh Ardekani, 2013), which implies that GPR is capable of characterizing the spatio-temporal SWC distribution at the field scale (e.g., Steelman et al., 2012).

In general, GPR measurements can be performed off the ground surface (off-ground GPR) (e.g., Lambot et al., 2004), on the soil surface (surface GPR) (e.g., van Overmeeren et al., 1997; Huisman et al., 2002) or in vertical or horizontal boreholes (borehole GPR) (e.g., Redman et al., 2000). Off-ground GPR relies on the use of an ultra-wide frequency band for subsurface investigations, and hence can potentially provide high-resolution information about the soil states. However, off-ground GPR measurements are influenced by surface roughness and only have a limited penetration

depth (Lambot et al., 2006a). For surface GPR measurements, SWC can be estimated based on the analysis of the direct ground wave (Grote et al., 2003; Weihermüller et al., 2007) or reflected waves (Lunt et al., 2005). Both GPR acquisition strategies have been successfully used to monitor water flow dynamics in unsaturated soil (Mangel et al., 2012; Moysey, 2010; Allroggen et al., 2015). The penetration depth of surface GPR is limited by the soil characteristics, especially by the bulk electric conductivity. Furthermore, there is no control on the vertical resolution when using reflected waves for SWC determination (Huisman et al., 2003). Borehole GPR can overcome these limitations but requires the availability and accessibility of appropriate boreholes or wells, and is therefore restricted to specialized test sites and experimental set-ups. Borehole GPR measurements have also been used to monitor SWC dynamics (Looms et al., 2008b). In addition, Zero-Offset-Profiling (ZOP) measurements between horizontal boreholes have been used to monitor SWC dynamics (Galagedara et al., 2002, Cai et al., 2016; Klotzsche et al., 2019a). Due to the good control on the vertical resolution and the improved spatial representativeness for the field plot scale, this kind of set-up provides detailed information on the spatial and temporal variation of SWC.

In order to derive soil hydraulic parameters from time-lapse GPR data, two types of inversion strategy can be used. The first type is commonly called sequential inversion and consists of three steps (Huisman et al., 2010; Hinnell et al., 2010). First, the dielectric permittivity ε is determined from the first arrival time of a GPR measurement using a straight-ray approximation (e.g., Galagedara et al., 2002) or a full-waveform inversion (e.g., Klotzsche et al., 2019b). Second, a petrophysical relationship is used to convert ε to SWC using the empirical Topp's equation (Topp et al., 1980) or a more

advanced dielectric mixing model (Roth et al., 1990). Third, the obtained time-lapse SWC data are used in combination with a hydrological model to estimate soil hydraulic parameters using inverse modelling. However, the use of a sequential inversion strategy may cause errors in the estimated soil hydraulic parameters when errors due to simplified geophysical data interpretations propagate into the estimated soil hydraulic parameters. An example of a potential source for such errors is the use of the straight-wave approximation for the travel path of the electromagnetic waves (Rucker and Ferré, 2004a). To overcome this problem, a coupled inversion strategy can be used (Hinnel et al., 2010; Lambot et al., 2006b). In contrast to sequential inversion, a coupled inversion links a hydrological model directly with a forward model of the geophysical data, and the mismatch between measured and modelled geophysical response is minimized (i.e. first arrival time or even the full waveform in the case of GPR). In doing so, the soil hydraulic parameters used in the hydrological model can be optimized, while error propagation is avoided. The coupled inversion approach relies heavily on an accurate forward hydrological model. A wrong conceptualization of the subsurface in terms of layering or processes not adequately captured by the hydrological model (e.g., dual porosity or macropore flow) will introduce errors that propagate into the estimated parameters.

A range of studies have employed off-ground GPR, surface GPR, and vertical borehole GPR measurements for estimating soil hydraulic properties from time-lapse SWC information by using either a sequential or a coupled inversion approach (e.g., Busch et al., 2013; Chen et al., 2001; Chen et al., 2004; Jadoon et al., 2012; Jaumann and Roth, 2018; Jonard et al., 2015; Kowalsky et al., 2005; Lambot et al., 2009; Rucker and Ferré,

2004b). Compared to these GPR acquisition strategies, horizontal borehole GPR measurements have several advantages to reveal the temporal and spatial SWC variations at the field plot scale. Firstly, horizontal borehole GPR measurements can provide SWC information at specific depths and thus have larger penetration depth and better control on vertical resolution compared to off-ground and surface GPR. Secondly, horizontal borehole GPR measurements provide a higher lateral spatial representativeness of the field plot compared to vertical borehole GPR measurements. However, no studies have been conducted yet that use horizontal borehole GPR measurements to parameterize a hydrological model. In this study, the performance of both sequential and coupled inversion workflows to obtain soil hydraulic properties from time-lapse horizontal borehole GPR data obtained during an infiltration event will be compared. To systematically study the differences between the two inversion approaches, a synthetic modelling experiment will be presented first. In a second step, actual horizontal borehole GPR measurements will be inverted using a coupled inversion approach. The resulting estimates of the hydraulic parameters will be compared to available independent hydraulic property estimates obtained from TDR measurements.

2. Material and methods

2.1 Test site and GPR data acquisition

An infiltration experiment was carried out on a bare soil plot at a rhizotron facility in Selhausen, Germany. In this facility, three plots (7 x 3 m) were established with different treatments (natural rain, rain-sheltered, and irrigated). GPR access tubes of 7 m length were horizontally installed at 0.1, 0.2, 0.4, 0.6, 0.8, and 1.2 m depth across the

entire length of the plot. The soil in the facility originates from fluvial gravel deposits from the Rur river system and is characterized as an Orthic Luvisol with high stone content (>50%) and a loamy texture (Table 1). Due to tillage activity, soil porosity Φ changes from 0.33 $cm^3\,cm^{-3}$ near the surface to approximately 0.25 $cm^3\,cm^{-3}$ below 0.3 m depth. In order to install the GPR access tubes, the entire plot was dug out and refilled layer-wise. Therefore, no pedogenetic horizons are detectable anymore below the plough horizon. No clear pedogenetic layers are detectable in the gravely layers of the natural soil either. For more information about the rhizotron facility, the reader is referred to Cai et al. (2016) and Klotzsche et al. (2019a).

The infiltration experiment consisted of five infiltration events that were carried out at the rain-sheltered plot during a 4-day period (Kelter et al., 2018). The experimental set-up, GPR data acquisition, and GPR data analysis were reported in Yu et al. (2020) in detail. Therefore, only a short summary is provided here. Water was infiltrated using a drip irrigation system that was supplied by water from an underground tank at a constant rate (0.03 cm min^{-1}). Approximately 2.7 cm of water was applied for each infiltration event of 90 min (Fig. 1a). ZOP surveys were made using a GPR system (PulseEKKO, Sensors & Software, Canada) with 200 MHz borehole antenna. GPR measurements were made at six depths (0.1, 0.2, 0.4, 0.6, 0.8 and 1.2 m) before and after infiltration events. During the infiltration events, GPR measurements were restricted to the boreholes at 0.1, 0.2 and 0.4 m depth as the SWC was expected to increase mainly at shallow depths at the beginning of each infiltration event. For each ZOP survey, the transmitter and receiver were first pushed to the end of the borehole (7 m) and then pulled simultaneously throughout the boreholes in 0.05 m steps. The survey

ended at 1.5 m distance from the access trench to avoid that reflections from the trench wall and installed sensors interfered with the direct waves.

The development of the mean GPR travel time at different depths is shown in Fig. 1b. To determine the GPR travel time from the ZOP data, the time-zero offset (T_0) and first arrival time (t^{obs}) of the direct wave were determined using the strategy proposed by Klotzsche et al. (2019a). In this strategy, T_0 was determined from wide angle reflection and refraction (WARR) measurements with the borehole antennae in air and t^{obs} was manually picked for each trace. GPR travel times measured at 0.1 and 0.2 m depth increased after the first infiltration event. In response to the second infiltration event, travel times up to a depth of 0.8 m responded to the infiltration. After the third infiltration event, the travel times increased at all depths. The standard deviation of the travel times is also shown in in Fig. 1b, which illustrates the spatial variability along the 5.5 m borehole tubes that were generated by the expected differences in the irrigation rate of the used dripping system and small-scale lateral water content variations caused by the heterogeneity of the soil. Based on the straight-ray approximation and independent of SWC, the observed ± 0.5 ns for the standard deviation of the travel time would lead to an uncertainty of ± 0.025 cm^3cm^{-3} for SWC.

Based on the known distance between the horizontal boreholes (d = 0.75 m), a 1D dielectric permittivity profile (ε^{obs}) can be calculated from the measured GPR travel times using:

$$\varepsilon^{obs} = \left[\frac{c*(t^{obs}-T_0)}{d}\right]^2 \quad (1)$$

where c is the speed of light in vacuum (0.3 m ns^{-1}). SWC (θ^{obs}) was calculated from

183 ε^{obs} using the complex refractive index model (CRIM) (Roth et al., 1990):

184 $$\theta^{obs} = \frac{\sqrt{\varepsilon^{obs}} - (1-\Phi)\sqrt{\varepsilon_s} - \Phi}{\sqrt{\varepsilon_w} - 1} \quad (2)$$

185 where ε_w is the permittivity of water (84 at 10°C), Φ is the porosity of the respective
186 layer, and ε_s is the permittivity of the solid soil fraction, which was assumed to be 4.7
187 for this facility, as considered by Klotzsche et al. (2019a). This value was also
188 suggested by Robinson et al. (2005) for soil with high quartz content, as is the case for
189 this facility.

190

191 *2.2 Hydrological modelling*

192 Vertical SWC dynamics during the infiltration experiment were simulated using
193 HYDRUS-1D (Šimůnek et al., 2008), which calculates one-dimensional variably-
194 saturated water flow by solving the Richards equation:

195 $$\frac{\partial \theta}{\partial t} = \frac{\partial}{\partial z}\left[K(h)\left(\frac{\partial h}{\partial z} + 1\right)\right] \quad (3)$$

196 where h is the pressure head (cm), θ is the volumetric water content ($cm^3\ cm^{-3}$), t is
197 time (min), z refers to the positive upward spatial coordinate (cm), and K is the
198 hydraulic conductivity ($cm\ min^{-1}$) as a function of h. $\theta(h)$ is the water retention
199 function described by the van Genuchten model (van Genuchten, 1980):

200 $$\theta(h) = \begin{cases} \theta_r + \frac{\theta_s - \theta_r}{(1+|\alpha h|^n)^m} & , h < 0 \\ \theta_s & , h \geq 0 \end{cases} \quad (4)$$

201 where θ_r is the residual water content ($cm^3\ cm^{-3}$), θ_s is the saturated water content (cm^3
202 cm^{-3}), α (cm^{-1}) is the inverse of the air-entry value, n is the pore-size distribution index
203 (-) and m is related to n by $m = 1 - 1/n$. The unsaturated hydraulic conductivity
204 $K_r(h)$ is given by:

$$K_r(h) = K_s S_e^l [1 - (1 - S_e^{1/m})^m]^2 \quad (5)$$

$$S_e = \frac{\theta - \theta_r}{\theta_s - \theta_r} \quad (6)$$

where K_s (cm min^{-1}) is the saturated hydraulic conductivity, S_e (-) is the effective saturation governed by Eq. 6 and l (-) is the tortuosity, which is generally set to 0.5 but can also be estimated for individual soils (e.g., Schaap and Leij, 2000). Using this Mualem – van Genuchten parameterization (Mualem, 1976; van Genuchten, 1980), the soil hydraulic properties are described by five parameters (i.e. K_s, θ_s, θ_r, α, and n).

For the simulation of vertical SWC dynamics, the model domain was set to be 150 cm deep and was discretized with 151 nodes with an equal spacing of 1 cm. Simulations were initialized using linearly interpolated SWC estimates from measured permittivity obtained from borehole GPR data acquired prior to the first infiltration event. Evaporation and root water uptake were both neglected in the simulation, as evaporation was low with respect to the amount of infiltrated water and the soil was bare. An atmospheric boundary condition with surface run-off was used to represent the irrigation events at the upper boundary of the domain. At the lower boundary of the domain, a seepage face (h = 0) was used. The use of a seepage face was required to match SWC observations and avoid excessive drainage out of the profile, which occurred when a free drainage boundary condition was used. A physical explanation for the need to use a seepage face may be the presence of a compacted soil layer directly below the rhizotron facility caused by the construction of the facility. As an alternative to the use of a seepage face, a longer soil profile with a dense layer with low K_s could have been used. However, this would have made the hydrological simulations computationally more demanding, especially in the case of the coupled inversion.

2.3 GPR modeling

The gprMax3D model was used to simulate GPR wave propagation with a Finite-Difference Time-Domain (FDTD) numerical method (Giannopoulos, 2005; Warren et al., 2016). The size of the simulation domain for the gprMax3D simulation was set to 2 x 1.1 x 2.2 m, including a soil of 1.5 m thickness below an air layer of 0.7 m. The 3D domain was discretized with nodes with 0.02 m spacing and perfectly matched layers (PML) were used at the boundaries of the model domain (Berenger, 1994). The center frequency of the antenna was set to 200 MHz (i.e. the center frequency of the antenna) and the first derivative of a Gaussian waveform was selected as the excitation function for the current source. As we only considered the velocity information for the GPR data interpretation, the electric conductivity of the soil was assumed to be zero.

2.4 Set-up for sequential and coupled inversion

To estimate hydraulic parameters from horizontal borehole GPR measurements, both sequential and coupled inversion strategies were used. The general set-ups of the two inversion strategies are illustrated in Fig. 2a and Fig. 2b. A key difference between the two approaches is that the sequential inversion approach directly optimizes the misfit between the SWC obtained from the GPR measurements (θ^{obs}) and the simulated SWC (θ^{mod}) provided by HYDRUS-1D, whereas the coupled inversion optimizes the misfit between the travel time of the measured GPR data (t^{obs}) and the simulated travel time (t^{mod}) obtained with gprMax3D using SWC information (θ^{mod}) provided by HYDRUS-1D. The misfits for the sequential and coupled inversions were described using cost functions based on the root-mean-square error (RMSE) between observed

and simulated data:

$$C_{MVG}(\theta) = \sqrt{\frac{\sum_{i=1}^{n}(\theta_i^{mod} - \theta_i^{obs})^2}{n}} \quad (7)$$

$$C_{MVG}(t) = \sqrt{\frac{\sum_{i=1}^{n}(t_i^{mod} - t_i^{obs})^2}{n}} \quad (8)$$

where n is the number of GPR measurements.

In order to minimize these cost functions, the Shuffled Complex Evolution (SCE-UA) algorithm introduced by Duan et al. (1993) was used. SCE-UA is a global optimization algorithm that not only has been widely used in hydrological research (e.g., Chu et al., 2010; Thyer and Kuczera, 1999) but also in geophysical applications (e.g., Liu et al., 2018; Mangel et al., 2017). The SCE-UA algorithm requires the specification of parameter bounds for each parameter considered in the optimization. The optimization includes several steps. First, different sets of hydraulic parameters are randomly created in the feasible parameter space and the cost function value for each of these parameter sets is calculated. Second, the parameter sets are sorted in order of their cost function value and distributed into several complexes that are subsequently evolved using the competitive complex evolution (CCE) algorithm (Duan et al., 1994). After this first loop of evolution, the complexes are merged again into a single population, which again is sorted in order of increasing cost function value and divided into complexes for the next optimization loop. The algorithm is considered to be converged if the cost function valued reaches a specified value (i.e. the known error of the data) or if the improvement in the best model is below 0.01% in the last 10 evolution loops.

Since no GPR measurements were made in dry soil conditions, the inversion is not

expected to be sensitive to θ_r. In order to build an independent hydrological model based on GPR measurement, θ_r was fixed it to 0 for the inversion and only K_s, θ_s, α, and n were estimated. K_s was inverted by using its log-transform ($\log(K_s)$). The algorithms for both sequential and coupled inversion were coded in GNU Octave (Eaton, 2012).

2.5 Set-up for synthetic infiltration experiments

2.5.1 Set-up for a 1-layer soil profile

Synthetic model experiments were performed to gain further insight into the feasibility of obtaining plausible parameter estimates from sequential and coupled inversion of time-lapse borehole GPR data. In a first model experiment, a 1-layer soil profile was considered. We used the soil hydraulic parameters for the top soil (0 - 30 cm) determined by Cai et al. (2017), which were estimated from TDR measurements at the same depths as the GPR access tubes (Table 2). In order to generate synthetic data for the model experiments, five infiltration events were simulated with an infiltration rate of 0.03 cm min^{-1}, which corresponds with the infiltration rate used in the actual field experiment. Since the 1-layer soil profile was constructed using the hydraulic parameters of the topsoil (higher θ_s), the amount of applied water was increased in the synthetic modelling experiment. In particular, the first three irrigation events now lasted 400 min whereas the last two infiltration events still lasted 90 min. After obtaining the SWC profile (θ^{mod}) from HYDRUS-1D, a dielectric permittivity profile (ε^{mod}) was calculated using the rearranged form of the CRIM model given in Eq. 2:

$$\varepsilon^{mod} = [(\sqrt{\varepsilon_w} - 1) * \theta^{mod} + (1 - \Phi) * \sqrt{\varepsilon_s} + \Phi]^2 \quad (9)$$

This dielectric permittivity profile was then used to simulate GPR measurements for the

six depths using gprMax3D.

2.5.2 Set-up for a 2-layer soil profile

A synthetic modelling experiment with a 2-layer soil profile was also performed. Sequential and coupled inversions for the 2-layer soil profile were conducted based on the infiltration schedule of the actual experiment (Fig. 1a). The hydraulic parameters in this second experiment were also based on Cai et al. (2017). However, the saturated hydraulic conductivity of the subsoil (K_{s2}) was changed from 0.0004 cm min^{-1} reported by Cai et al. (2017) to 0.04 cm min^{-1}, because it had to be larger than the infiltration rate of 0.03 cm min^{-1} to avoid ponding of water at the layer interface. For a more realistic synthetic modelling study, Gaussian noise with zero mean and a standard deviation of 0.1 ns and 0.01 cm^3 cm^{-3} was added to the synthetic travel times and SWC data, respectively, for both the 1-layer and the 2-layer model.

2.5.3 Automatic picking of the first arrival time

The implementation of the coupled inversion approach requires an automatic picking of the first arrival time. For the simulated GPR data, the first arrival time can be automatically determined using an amplitude threshold. To obtain this threshold, the excitation moment (T_s) of the simulated data was determined from the onset of the source wavelet. The source wavelet is defined as the first derivative of the Gaussian waveform:

$$I = -2\zeta\sqrt{e^{\frac{1}{2\zeta}}e^{-\zeta(t-\chi)^2}}(t-\chi) \quad (10)$$

where $\zeta = 2\pi^2 f^2$ and $\chi = 1/f$, I is the electric current density (A m^{-2}), e is the natural

logarithm, and f is the center frequency of the antenna (200 MHz). From this source wavelet, a T_s of 1.62 ns was manually determined (Fig. 3a). Subsequently, an air wave was simulated using antennas positioned at 0.1 m above the ground surface (Fig. 3b). With the known propagation velocity in air (0.3 m ns^{-1}) and the antenna separation (0.75 m), the true travel time of the air wave is 2.5 ns. The appropriate amplitude threshold (0.0158 V m^{-1}) was then determined from the amplitude of the simulated air wave at the travel time of 4.12 ns, which is the sum of T_s (1.62 ns) and true travel time of the air wave (2.5 ns).

To verify the robustness of the automatic first arrival time determination, a synthetic infiltration-induced SWC profile was generated by HYDRUS-1D (Fig. 3c) and ZOP measurements were simulated using gprMax3D at different depths. The amplitude threshold of 0.0158 V m^{-1} was used to determine the first arrival time (Fig. 3d). It was found that the amplitude of the traces rapidly increased after the determined first arrival time, which confirms the robustness of automatic procedure for the determination of the first arrival time.

2.6 Uncertainty Analysis

Proper quantification of uncertainty in the estimated soil hydraulic parameters is of great importance given that the information content of soil water content measurements for the estimation of soil hydraulic properties depends on the initial and boundary conditions during the experiment (Mboh et al., 2011). In this study, we used both response surface analysis (Toorman et al., 1992) and a simple first-order approximation (Kool and Parker, 1988; Kuczera and Mroczkowski, 1998; Vrugt and Dane, 2006) to

investigate the uncertainty of the inverted hydraulic parameters.

Response surfaces provide a 2D view of the cost function distribution obtained with a grid search. In order to obtain such surfaces, two hydraulic parameters (e.g., α and n) are varied between defined bounds, whereas the other hydraulic parameters (e.g., $\log(K_s)$ and θ_s) are fixed at their true (or optimized) value. Response surfaces are a robust method to visualize parameter uncertainty and the minimum of the cost function. However, they commonly require a high computational effort, especially in the case of many model parameters (i.e. the 2-layer model). Therefore, this method was only used for the synthetic model study with a 1-layer soil profile.

A classic first-order approximation of parameter uncertainty was also used (Vrugt and Dane, 2006). It is based on the covariance matrix (C) of the optimized hydraulic parameters, which is calculated by:

$$C = s^2(J^T J)^{-1} \tag{11}$$

where s^2 is the error variance between simulated and observed data and J is the Jacobian matrix. The Jacobian matrix is the first-order partial derivative of the cost function for each inverted hydraulic parameter and was obtained using a finite difference approach. The marginal posterior distribution of the estimated hydraulic parameters (m^{est}) is assumed to be a multivariate normal distribution $N\ (m^{est}, C)$. The uncertainty of the estimated hydraulic parameters can be approximated by the confidence interval for a given level (i.e. 99%) of significance calculated from the diagonal elements of C. A matrix (A) that provides the correlation between the estimated hydraulic parameters can be obtained by dividing the elements of C with the

369 square root of the diagonal elements of C:

370 $$A_{ij} = \frac{c_{ij}}{c_{ii}^{1/2} c_{jj}^{1/2}} \quad (12)$$

371 This first-order approximation is an efficient way for estimating the uncertainty of the
372 estimated hydraulic parameters for linear or nearly linear hydrologic models and the
373 correlation matrix is a useful indicator of parameter correlation (Zhu and Mohanty,
374 2003). If the hydrological model is highly non-linear, the first-order approximation may
375 be unreliable. Therefore, we only focus on A_{ij} values larger than 0.6 in our analysis.

376

377 ## 3. Results and Discussion

378 ### *3.1 Synthetic infiltration experiments*

379 The simulated vertical SWC profiles at times where GPR measurements were obtained
380 are shown in Fig. 4 for the synthetic modelling study with a 1-layer soil. It can be seen
381 that the infiltration front moved down to 0.6 and 1.2 m depth after the first and second
382 infiltration event, respectively. After the third infiltration event, the entire soil profile
383 was saturated. Because of the high saturation after the third infiltration event, the
384 infiltration front moved rapidly downward through the entire soil profile during
385 infiltration events 4 and 5. The SWC estimates obtained from the first-arrival time of
386 simulated horizontal borehole GPR measurements using a straight-wave approximation
387 are also shown in Fig. 4b. It was found that SWC estimates obtained from GPR
388 measurements at shallow depth (0 – 0.2 m) and near the infiltration front underestimated
389 the actual SWC (Fig. 4b and 4c). This is attributed to the interference of the direct wave
390 with critical refractions generated at the air – soil interface and the infiltration front
391 where the dielectric permittivity changes sharply (Rucker and Ferré, 2004a). For this

reason, horizontal borehole GPR measurements at 0.1 m depth were previously not considered for SWC estimation (Klotzsche et al., 2019a). In the synthetic study, these data were also not used in the sequential inversion to reduce this interpretation error. Unfortunately, errors in SWC estimates near the infiltration front cannot be simply identified and eliminated and thus are expected to affect the estimated hydraulic parameters obtained with the sequential inversion approach. For the coupled inversion, the effect of the air-soil interface is considered in the simulation of GPR wave propagation and therefore there is no need to remove the measurement at 0.1 m depth. However, the information content with respect to the soil hydraulic properties is expected to be limited for these measurements because of the limited travel path length in the topsoil.

3.1.1 Response surfaces for the 1-layer soil profile

Fig. 5a presents the response surface based on true SWC data that would be obtained using point measurements (i.e. TDR) at the same depth as the borehole GPR measurements. The corresponding response surfaces for the noise-free coupled inversion of the synthetic GPR data are shown in Fig. 5b. It can be seen that the cost functions for point and GPR measurements have a very similar misfit distribution. This is not unexpected given that point and GPR measurements provide a similar type of information, albeit with a different sampling volume (Klotzsche et al., 2019a). The response surfaces can be used to gain insight in the expected parameter uncertainty. In the case of the α parameter, the response surfaces for $n - \alpha$, $\theta_r - \alpha$, and $\theta_s - \alpha$ indicate that changes in the cost function are parallel to the α axis. This suggests that the α parameter is independent from the other parameters. Although a clear minimum in the cost function value can be observed in these three surfaces, it is also elongated in the

direction of the α axis suggesting that the α parameter is expected to be less constrained in the inversion results compared to the other model parameters. According to the response surfaces for $\theta_s - n$ and $\theta_s - \log(K_s)$, estimates of θ_s are expected to be correlated with the estimates of n and $\log(K_s)$. In the vicinity of the global minimum, the response surface is almost perpendicular to the θ_s axis and steep, which suggests that θ_s estimates are well-constrained during inversion. The global minimum in the response surface between $\log(K_s)$ and n is positioned in an elongated valley. A strong negative correlation between the parameter estimates for $\log(K_s)$ and n is thus expected, which implies that the GPR measurements may not contain sufficient information to simultaneously constrain both $\log(K_s)$ and n.

3.1.2 Inversion results for the 1-layer soil profile

Sequential and coupled inversions were performed using noisy simulated GPR measurements for the 1-layer soil profile. In the case of the sequential inversion, the fitted SWC data showed a large misfit with the expected SWC (Fig. 6a), particularly for the shallow depths (0.2 m). This is also reflected in the large cost function value (0.05 cm^3 cm^{-3}) for the optimized parameters, which is much higher than the added uncertainty in the SWC data (0.01 cm^3 cm^{-3}). Additionally, the SWC profiles simulated by using the estimated parameters from the sequential inversion showed large deviation with the SWC profiles from the true forward model (Fig. 7a). Due to the poor fit to the data, the hydraulic parameters were not accurately estimated by the sequential inversion (Table 3). In particular, θ_s was strongly underestimated and this resulted in a large mismatch between the inverted and true water retention curves (Fig. 8a). Moreover, the estimated value for K_s was at the lower boundary of the feasible parameter space (0.035

cm min^{-1}), which is almost equal to the infiltration rate. The n and α parameters were also overestimated, which resulted in a large difference between the inverted and true relative hydraulic conductivity function (Fig. 8b). As detailed above, sequential inversion of ZOP data may lead to erroneous estimates of hydraulic parameters if strong vertical gradients in SWC are present (e.g. infiltration-induced gradients).

In the case of the parameters estimated from coupled inversion, the simulated travel time fitted the known travel time from the true model well (Fig. 6b) as expressed by the low RMSE of 0.1 ns. Also, the simulated SWC profiles matched well the SWC profiles from the true model (Fig. 7a). It should be noted that the coupled inversion was ended when the cost function value decreased to the standard deviation of the Gaussian noise (0.1 ns) (Table 3) to avoid overfitting. Therefore, the data simulated with the inverted model parameters have the same RMSE as the noise-free data and the simulated travel times based on the inverted parameters also match well with the noise-free data.

The values for θ_s and α were accurately estimated by coupled inversion (Table 3). However, the estimated values for n and $\log(K_s)$ showed a slight deviation from the true model, likely because of the strong correlation between these two parameters. The accurate estimation of the hydraulic parameters is also reflected in the good match between the estimated and known water retention and relative hydraulic conductivity function (Fig. 8a, 8b). The first-order uncertainty estimates for the coupled inversion are presented in Table 3 and the associated correlation matrix of the estimated hydraulic parameters is given in Table 4. The results indicate a strong negative correlation for $\log(K_s)$ - n and weak correlations between other pairs of hydraulic parameters. This is

consistent with the results of the response surface analysis and confirms that the first-order approximation provides a meaningful assessment of parameter uncertainty.

3.1.3 Inversion results for the 2-layer soil profile

In a next step, the synthetic modelling study for the two-layer soil profile was analyzed. As expected from the results of the 1-layer soil profile, the parameters estimated using sequential inversion deviated considerably from the true hydraulic parameters (Table 3) and the estimated and true water retention (Fig. 8c, 8e) and relative hydraulic conductivity functions did not match well (Fig. 8d, 8f). Hence, sequential inversion will not be considered for the analysis of the actual field measurements.

The results of the coupled inversion for the 2-layer soil profile generally were consistent with the results of the 1-layer profile, despite the dimensional expansion of the search space from four to eight parameters. Again, the estimated travel times from coupled inversion results nicely fitted the noisy synthetic travel time series (Fig. 9) and the vertical SWC profiles from the true model (Fig. 7b). In addition, accurate hydraulic parameter estimates were obtained (Table 3), as also confirmed by the minor differences in estimated and true water retention (Fig. 8c, 8e) and relative hydraulic conductivity functions (Fig. 8d, 8f).

3.2 Inversion of experimental GPR data

Coupled inversion was used to estimate the hydraulic parameters from the measured horizontal borehole GPR data shown in Fig. 10. The resulting fit to the measured data is also shown in Fig. 10 and the estimated soil hydraulic parameters are provided in Table

5. For comparison, the simulated data using the hydraulic parameters of Cai et al. (2017) are also provided, which are based on long-term TDR measurements also made during vegetation periods. The comparison between measured and simulated travel times showed a good correspondence at 0.1 m depth both for the inverted hydraulic parameters and the parameters from Cai et al. (2017) (Fig. 10). For 0.2 m depth, the measured GPR travel times steadily increased during the entire infiltration experiment, whereas the simulated travel times using both sets of hydraulic parameters remained constant after the second infiltration event because the soil reached saturation. This can be explained by the heterogeneous nature of the topsoil, which is supported by the large spatial variation of the GPR travel time data. For the subsoil, the key features of the measured time-lapse GPR data were well captured by the coupled inversion, also considering the spatial variability in the measured GPR data. The simulated travel time data based on the hydraulic parameters of Cai et al. (2017) did not match the observed GPR data well in the subsoil (i.e. at 0.6, 0.8, and 1.2 m depth). This is attributed to the small K_{s2} used in Cai et al. (2017), which results in a slow movement of the infiltration front in the subsoil (Fig. 11), and therefore, a reduced variation in simulated water content at large depths.

Measured and inverted GPR travel time data are directly compared in Fig. 12. The use of the hydraulic parameters from Cai et al. (2017) clearly resulted in a systematic underestimation of the measured data and a relatively high RMSE of 0.43 ns. The hydraulic parameters obtained using coupled inversion better matched the measured travel time data, as indicated by the lower RMSE (0.32 ns) and a higher R^2 value (0.90). Nevertheless, the RMSE between inverted and measured GPR data is still relatively

large. This is partly attributed to the heterogeneity of the topsoil, as the measurements at 0.2 m depth make up a considerable part of the observed misfit. Furthermore, there is uncertainty in the initial SWC profile, which is solely based on GPR measurements at six different depths. Here, extrapolation from the shallowest borehole to the soil surface is problematic, and may have introduced some degree of uncertainty. Finally, there is intrinsic uncertainty in the field GPR measurements and data processing, such as the uncertainty in the position of the horizontal boreholes and the uncertainty in the determination of the time-zero or first arrival time of measured GPR data. These issues obviously did not affect the coupled inversion in the synthetic case study but they are highly relevant for the inversion of actual field measurements.

The results of the first-order uncertainty estimation of the inverted hydraulic parameters are provided in Table 5. The uncertainty of α and θ_s are comparable for the top- and subsoil, whereas n and $\log(K_s)$ showed a larger uncertainty for the subsoil. This can be explained by the strong negative correlation (A = -0.615) between n_2 and $\log(K_{s2})$ (Table 6). All other pairs of hydraulic parameters did not show strong correlations. Fig. 13 presents the water retention and relative hydraulic conductivity functions obtained using coupled inversion. The associated uncertainty was obtained by randomly plotting 100 sets of hydraulic parameters drawn from the uncertainty bounds provided in Table 5. As can be seen from the uncertainty bounds, θ_s is associated with a relatively low uncertainty, whereas the n value is associated with a larger uncertainty as indicated by the increasing spread of the functions at lower pressure heads. Furthermore, uncertainty in the water retention function is similar for the top- and subsoil (Fig. 13a, 13c). For comparison, the functions based on the hydraulic parameters of Cai et al. (2017) were

534 also provided. The water retention function obtained using coupled inversion clearly
535 deviated from that of Cai et al. (2017), which showed a faster decrease of water content
536 with matric potential due to the larger n value. Additionally, a lower θ_s was estimated
537 by the coupled inversion.
538
539 The hydraulic conductivity functions obtained using coupled inversion also showed a
540 similar uncertainty for the top- and subsoil (Fig. 13b, 13d). For the topsoil, the hydraulic
541 conductivity function obtained using coupled inversion corresponded well with the
542 function obtained in Cai et al. (2017). This is at least partly due to the similarity in the
543 inverted K_s obtained in this study and in Cai et al. (2017). However, there are obvious
544 differences in the hydraulic conductivity functions for the subsoil due to differences in
545 estimated K_s. There is a range of possible explanations for the observed differences.
546 First, the estimation of K_s is known to be scale-dependent. For example, laboratory
547 methods using small sample volumes often lead to lower K_s compared to estimates from
548 in-situ measurement from a larger soil volume (Busch et al., 2013; Rovey and
549 Cherkauer, 1995). The results of Cai et al. (2017) were based on TDR measurement that
550 only cover a small areal fraction of the rhizotron facility, whereas the GPR
551 measurements represent a larger volume (Klotzsche et al., 2019a). Thus, a higher K_s is
552 perhaps expected for the GPR measurements since the importance of preferential flow
553 in macropores likely increased from the TDR to the GPR scale. The analysis presented
554 here also indicated potential parameter correlations between K_s and n. Since larger n
555 values were reported by Cai et al. (2017), this may explain the small K_s values. It is also
556 important to note that Cai et al. (2017) estimated hydraulic parameters with a more
557 complex model set-up that considered root water uptake. In particular, root water uptake

parameters were estimated alongside the hydraulic parameters, which might have hampered the correct estimation of the soil hydraulic parameters and likely increased the uncertainty in the estimated hydraulic parameters obtained by Cai et al. (2017). Finally, it is important to note that Cai et al. (2017) assumed free drainage as a lower boundary condition whereas a seepage face was used in this study.

4. Summary and Conclusions

In this study, we used both sequential and coupled inversion strategies to estimate hydraulic parameters from horizontal borehole GPR measurements during an infiltration experiment. First, a synthetic modelling study was set-up to compare the two inversion approaches independent of measurement and model errors. In a noise-free synthetic study using a 1-layer soil profile, a response surface analysis was used to evaluate correlation between hydraulic parameters. The results showed that the hydraulic parameters n and $\log(K_s)$ were strongly correlated, which implies that the GPR measurements were not able to simultaneously constrain $\log(K_s)$ and n. In a next step, synthetic SWC and travel time data with added noise were used to estimate hydraulic parameters using sequential and coupled inversion approaches, respectively. It was observed that a sequential inversion approach relying on the conventional straight-ray approximation to estimate SWC did not provide accurate hydraulic parameter estimates if strong vertical gradients in SWC were present due to infiltration. The coupled inversion approach, which combined 3D modelling of GPR measurements with a 1D vadose zone flow model, was able to provide accurate estimates of the hydraulic parameters both for a 1-layer and a 2-layer soil profile because interpretation errors associated with the straight-ray approximation were avoided. In a final step, horizontal

582 borehole GPR measurements made during an infiltration experiment were inverted
583 using a coupled inversion approach. The estimated hydraulic parameters were
584 reasonably consistent with water retention and relative hydraulic conductivity functions
585 reported by Cai et al. (2017) for the same site.
586
587 In conclusion, the coupled inversion of horizontal borehole GPR measurements
588 provided accurate field-scale estimates of soil hydraulic parameters. Because of the
589 larger sampling volume compared to point sensors, the estimated hydraulic parameters
590 are expected to have an improved field representativeness. In future studies, coupled
591 inversion of horizontal borehole GPR data may be used to estimate 2D and perhaps
592 even 3D distributions of soil hydraulic parameters by considering all measured travel
593 times over the profile, although this will obviously be associated with a higher
594 computational effort. A disadvantage of the proposed approach is that GPR
595 measurements are still taken manually and are thus time-consuming, whereas point
596 sensors often allow automated data acquisition. As an alternative to GPR, other
597 geophysical methods such as ERT can also be employed to estimate hydraulic
598 parameters. ERT can investigate the subsurface with high resolution, and data
599 acquisition can be automated. However, the electrical conductivity distribution obtained
600 with ERT is not only sensitive to SWC but also depends on several other factors (e.g.,
601 clay content, pore water salinity) (Binley et al., 2015). This can complicate vadose zone
602 model parameterization using ERT measurements considerably. It would be interesting
603 to extend coupled inversion by considering the full GPR waveform instead of solely
604 using travel time information, as was recently proposed for seismic data by Li et al.
605 (2020). It is expected that this would increase the information content of the GPR

measurements in the inversion, and therefore reduce uncertainty in the estimated hydraulic parameters and provide chances to estimate hydraulic properties of multi-layer soils.

Acknowledgements

The first author is supported by a CSC scholarship [grant number: No. 201606410058]. This work has partially been funded by the German Research Foundation (Deutsche Forschungsgemeinschaft, DFG) under Germany's Excellence Strategy, EXC-2070 - 390732324 – PhenoRob, and the SFB/TR32 "Patterns in Soil-Vegetation-Atmosphere Systems: monitoring, modelling, and data assimilation". The rhizotron facility is supported by TERENO (Terrestrial Environmental Observations) funded by the Helmholtz-Gemeinschaft. The authors gratefully acknowledge the computing time granted by the John von Neumann Institute for Computing (NIC) and provided on the supercomputer JURECA (Jülich Supercomputing Centre, 2018) of the Jülich Supercomputing Centre (JSC).

References

Abbaspour, K., Kasteel, R., Schulin, R., 2000. Inverse parameter estimation in a layered unsaturated field soil. Soil Sci. 165(2): 109-123.

Allroggen, N., van Schaik, N.L.M.B., Tronicke, J., 2015. 4D ground-penetrating radar during a plot scale dye tracer experiment. J. Appl. Geophy. 118: 139-144. doi:10.1016/j.jappgeo.2015.04.016

Berenger, J.-P., 1994. A perfectly matched layer for the absorption of electromagnetic waves. J. Comput. Phys. 114(2): 185-200. doi:10.1006/jcph.1994.1159

Binley, A., Hubbard, S.S., Huisman, J.A., Revil, A., Robinson, D.A., Singha, K., Slater, L.D., 2015. The emergence of hydrogeophysics for improved understanding of subsurface processes over multiple scales. Water Resour. Res. 51(6): 3837-3866. doi: 10.1002/2015WR017016

Blanco-Canqui, H., Lal, R., 2007. Impacts of long-term wheat straw management on soil hydraulic properties under no-tillage. Soil Sci. Soc. Am. J. 71(4): 1166-1173. doi:10.2136/sssaj2006.0411

Brosten, T.R., Day-Lewis, F.D., Schultz, G.M., Curtis, G.P., Lane, J.W., 2011. Inversion of multi-frequency electromagnetic induction data for 3D characterization of hydraulic conductivity. J. Appl. Geophy. 73(4): 323-335. doi:https://doi.org/10.1016/j.jappgeo.2011.02.004

Brunet, P., Clément, R., Bouvier, C., 2010. Monitoring soil water content and deficit using Electrical Resistivity Tomography (ERT) – A case study in the Cevennes area,

644 France. J. Hydrol. 380(1): 146-153. doi:10.1016/j.jhydrol.2009.10.032

645 Busch, S., Weihermüller, L., Huisman, J.A., Steelman, C.M., Endres, A.L., Vereecken,
646 H., van der Kruk, J., 2013. Coupled hydrogeophysical inversion of time-lapse surface
647 GPR data to estimate hydraulic properties of a layered subsurface. Water Resour. Res.
648 49(12): 8480-8494. doi:10.1002/2013wr013992

649 Cai, G., Vanderborght, J., Couvreur, V., Mboh, C.M., Vereecken, H., 2017.
650 Parameterization of root water uptake models considering dynamic root distributions
651 and water uptake compensation. Vadose Zone J. 17(1): 160125.
652 doi:10.2136/vzj2016.12.0125

653 Cai, G., Vanderborght, J., Klotzsche, A., van der Kruk, J., Neumann, J., Hermes, N.,
654 Vereecken, H., 2016. Construction of minirhizotron facilities for investigating root
655 zone processes. Vadose Zone J. 15(9): 1-13. doi:10.2136/vzj2016.05.0043

656 Chanasyk, D.S., Naeth, M.A., 1996. Field measurement of soil moisture using neutron
657 probes. Can. J. Soil Sci. 76(3): 317-323. doi:10.4141/cjss96-038

658 Chen, J., Hubbard, S., Rubin, Y., 2001. Estimating the hydraulic conductivity at the
659 south oyster site from geophysical tomographic data using Bayesian techniques based
660 on the normal linear regression model. Water Resour. Res. 37(6): 1603-1613.
661 doi:10.1029/2000wr900392

662 Chen, J., Hubbard, S., Rubin, Y., Murray, C., Roden, E., Majer, E., 2004. Geochemical
663 characterization using geophysical data and Markov Chain Monte Carlo methods: A
664 case study at the South Oyster bacterial transport site in Virginia. Water Resour. Res.
665 40(12). doi:10.1029/2003wr002883

666 Chu, W., Gao, X., Sorooshian, S., 2010. Improving the shuffled complex evolution
667 scheme for optimization of complex nonlinear hydrological systems: Application to
668 the calibration of the Sacramento soil-moisture accounting model. Water Resour. Res.
669 46(9). doi:10.1029/2010wr009224

670 Duan, Q., Sorooshian, S., Gupta, V.K., 1994. Optimal use of the SCE-UA global
671 optimization method for calibrating watershed models. J. Hydrol. 158(3): 265-284.
672 doi:10.1016/0022-1694(94)90057-4

673 Duan, Q.Y., Gupta, V.K., Sorooshian, S., 1993. Shuffled complex evolution approach
674 for effective and efficient global minimization. J. OPTIMIZ. THEORY. APP. 76(3):
675 501-521. doi:10.1007/BF00939380

676 Eaton, J.W., 2012. GNU Octave and reproducible research. J. Process Control. 22(8):
677 1433-1438. doi:10.1016/j.jprocont.2012.04.006

678 Galagedara, L., Parkin, G., Redman, J., Endres, A., 2002. Temporal and spatial
679 variation of soil water content measured by borehole GPR under irrigation and
680 drainage, Ninth International Conference on Ground Penetrating Radar (GPR2002).
681 SPIE, pp. 180–185. doi:10.1117/12.462253.

682 Giannopoulos, A., 2005. Modelling ground penetrating radar by GprMax. Constr. Build
683 Mater. 19(10): 755-762. doi:10.1016/j.conbuildmat.2005.06.007

684 Grote, K., Hubbard, S., Rubin, Y., 2003. Field-scale estimation of volumetric water
685 content using ground-penetrating radar ground wave techniques. Water Resour. Res.
686 39(11). doi:10.1029/2003wr002045

687 Hartmann, A., Goldscheider, N., Wagener, T., Lange, J., Weiler, M., 2014. Karst water
688 resources in a changing world: Review of hydrological modeling approaches. Rev.
689 Geophys. 52(3): 218-242. doi:10.1002/2013rg000443

690 Hinnell, A.C., Ferré, T.P.A., Vrugt, J.A., Huisman, J.A., Moysey, S., Rings, J.,
691 Kowalsky, M.B., 2010. Improved extraction of hydrologic information from
692 geophysical data through coupled hydrogeophysical inversion. Water Resour. Res.
693 46(4). doi:10.1029/2008wr007060

694 Holliger, K., Musil, M., Maurer, H.R., 2001. Ray-based amplitude tomography for
695 crosshole georadar data: a numerical assessment. J. Appl. Geophy. 47(3): 285-298.
696 doi:10.1016/S0926-9851(01)00072-6

697 Hubbard, S.S., Rubin, Y., 2000. Hydrogeological parameter estimation using
698 geophysical data: a review of selected techniques. J. Contam. Hydrol. 45(1): 3-34.
699 doi:10.1016/S0169-7722(00)00117-0

700 Huisman, J.A., Hubbard, S.S., Redman, J.D., Annan, A.P., 2003. Measuring soil water
701 content with ground penetrating radar: A Review. Vadose Zone J. 2(4): 476-491.
702 doi:10.2136/vzj2003.4760

703 Huisman, J.A., Rings, J., Vrugt, J.A., Sorg, J., Vereecken, H., 2010. Hydraulic
704 properties of a model dike from coupled Bayesian and multi-criteria hydrogeophysical
705 inversion. J. Hydrol. 380(1): 62-73. doi:10.1016/j.jhydrol.2009.10.023

706 Huisman, J.A., Snepvangers, J.J.J.C., Bouten, W., Heuvelink, G.B.M., 2002. Mapping
707 spatial variation in surface soil water content: comparison of ground-penetrating radar
708 and time domain reflectometry. J. Hydrol. 269(3): 194-207. doi:10.1016/S0022-

709 1694(02)00239-1

710 Jadoon, K.Z., Weihermüller, L., Scharnagl, B., Kowalsky, M.B., Bechtold, M., Hubbard,
711 S.S., Vereecken, H., Lambot, S., 2012. Estimation of soil hydraulic parameters in the
712 field by integrated hydrogeophysical inversion of time-lapse ground-penetrating radar
713 data. Vadose Zone J. 11(4): vzj2011.0177. doi:10.2136/vzj2011.0177

714 Jaumann, S., Roth, K., 2018. Soil hydraulic material properties and layered architecture
715 from time-lapse GPR. Hydrol. Earth Syst. Sci. 22(4): 2551-2573. doi:10.5194/hess-22-
716 2551-2018

717 Jonard, F., Weihermüller, L., Schwank, M., Jadoon, K.Z., Vereecken, H., Lambot, S.,
718 2015. Estimation of Hydraulic Properties of a Sandy Soil Using Ground-Based Active
719 and Passive Microwave Remote Sensing. IEEE Trans. Geosci. Remote Sens. 53(6):
720 3095-3109. doi:10.1109/TGRS.2014.2368831

721 Jülich Supercomputing Centre, 2018. Jureca: Modular supercomputer at Jülich
722 Supercomputing Centre. J. Large-Scale Res. Fac. 4: 132. doi:10.17815/jlsrf-4-121-1

723 Katul, G.G., Wendroth, O., Parlange, M.B., Puente, C.E., Folegatti, M.V., Nielsen, D.R.,
724 1993. Estimation of in situ hydraulic conductivity function from nonlinear filtering
725 theory. Water Resour. Res. 29(4): 1063-1070. doi:10.1029/92wr02593

726 Kelter, M., Huisman, J.A., Zimmermann, E., Vereecken, H., 2018. Field evaluation of
727 broadband spectral electrical imaging for soil and aquifer characterization. J. Appl.
728 Geophy. 159: 484-496. doi:10.1016/j.jappgeo.2018.09.029

729 Klotzsche, A., Jonard, F., Looms, M.C., van der Kruk, J., Huisman, J.A., 2018.

730 Measuring soil water content with ground penetrating radar: A decade of progress.
731 Vadose Zone J. 17(1): 180052. doi:10.2136/vzj2018.03.0052

732 Klotzsche, A., Lärm, L., Vanderborght, J., Cai, G., Morandage, S., Zörner, M.,
733 Vereecken, H., van der Kruk, J., 2019a. Monitoring soil water content using time-lapse
734 horizontal borehole GPR data at the field-plot scale. Vadose Zone J. 18(1): 190044.
735 doi:10.2136/vzj2019.05.0044

736 Klotzsche, A., Vereecken, H., van der Kruk, J, 2019b. Review of crosshole ground-
737 penetrating radar full-waveform inversion of experimental data: Recent developments,
738 challenges, and pitfalls. GEOPHYSICS. 84(6): H13-H28. doi:10.1190/geo2018-
739 0597.1

740 Kuczera, G., Mroczkowski, M., 1998. Assessment of hydrologic parameter uncertainty
741 and the worth of multiresponse data. Water Resour. Res. 34(6): 1481-1489.
742 doi:10.1029/98WR00496

743 Klute, A., Dirksen, C., 1986. Hydraulic conductivity and diffusivity: Laboratory
744 methods. Methods of Soil Analysis: Part 1 Physical and Mineralogical Methods. 5:
745 687-734.

746 Kool, J.B., Parker, J.C., 1988. Analysis of the inverse problem for transient unsaturated
747 flow. Water Resour. Res. 24(6): 817-830. doi:10.1029/WR024i006p00817

748 Kool, J.B., Parker, J.C., van Genuchten, M.T., 1987. Parameter estimation for
749 unsaturated flow and transport models — A review. J. Hydrol. 91(3): 255-293.
750 doi:10.1016/0022-1694(87)90207-1

751 Kowalsky, M.B., Finsterle, S., Peterson, J., Hubbard, S., Rubin, Y., Majer, E., Ward, A.,
752 Gee, G., 2005. Estimation of field-scale soil hydraulic and dielectric parameters
753 through joint inversion of GPR and hydrological data. Water Resour. Res. 41(11).
754 doi:10.1029/2005wr004237

755 Kumar, S., Sekhar, M., Reddy, D.V., Mohan Kumar, M.S., 2010. Estimation of soil
756 hydraulic properties and their uncertainty: comparison between laboratory and field
757 experiment. Hydrol. Process. 24(23): 3426-3435. doi:10.1002/hyp.7775

758 Lambot, S., Antoine, M., Vanclooster, M., Slob, E.C., 2006a. Effect of soil roughness
759 on the inversion of off-ground monostatic GPR signal for noninvasive quantification
760 of soil properties. Water Resour. Res. 42(3). doi:10.1029/2005wr004416

761 Lambot, S., Slob, E.C., Vanclooster, M., Vereecken, H., 2006b. Closed loop GPR data
762 inversion for soil hydraulic and electric property determination. Geophys. Res. Lett.
763 33(21). doi:10.1029/2006GL027906

764 Lambot, S., Rhebergen, J., van den Bosch, I., Slob, E.C., Vanclooster, M., 2004.
765 Measuring the soil water content profile of a sandy soil with an off-ground monostatic
766 ground penetrating radar. Vadose Zone J. 3(4): 1063-1071. doi:10.2136/vzj2004.1063

767 Lambot, S., Slob, E., Rhebergen, J., Lopera, O., Jadoon, K.Z., Vereecken, H., 2009.
768 Remote estimation of the hydraulic properties of a sand using full-waveform integrated
769 hydrogeophysical inversion of time-Lapse, off-Ground GPR data. Vadose Zone J. 8(3):
770 743-754. doi:10.2136/vzj2008.0058

771 Li, D., Xu, K., Harris, J.M., Darve, E., 2020. Coupled Time-Lapse Full-Waveform
772 Inversion for Subsurface Flow Problems Using Intrusive Automatic Differentiation.

773 Water Resour. Res. 56(8): e2019WR027032. doi:10.1029/2019wr027032

774 Liu, T., Klotzsche, A., Pondkule, M., Vereecken, H., Su, Y., Kruk, J.v.d., 2018. Radius
775 estimation of subsurface cylindrical objects from ground-penetrating-radar data using
776 full-waveform inversion. GEOPHYSICS. 83(6): H43-H54. doi:10.1190/geo2017-
777 0815.1

778 Looms, M.C., Binley, A., Jensen, K.H., Nielsen, L., Hansen, T.M., 2008a. Identifying
779 unsaturated hydraulic parameters using an integrated data fusion approach on cross-
780 borehole geophysical data. Vadose Zone J. 7(1): 238-248. doi:10.2136/vzj2007.0087

781 Looms, M.C., Jensen, K.H., Binley, A., Nielsen, L., 2008b. Monitoring unsaturated
782 flow and transport using cross-borehole geophysical methods. Vadose Zone J. 7(1):
783 227-237. doi:10.2136/vzj2006.0129

784 Lunt, I.A., Hubbard, S.S., Rubin, Y., 2005. Soil moisture content estimation using
785 ground-penetrating radar reflection data. J. Hydrol. 307(1): 254-269.
786 doi:10.1016/j.jhydrol.2004.10.014

787 Mahmoudzadeh Ardekani, M.R., 2013. Off- and on-ground GPR techniques for field-
788 scale soil moisture mapping. Geoderma. 200-201: 55-66.
789 doi:10.1016/j.geoderma.2013.02.010

790 Malicki, M.A., Plagge, R., Renger, M., Walczak, R.T., 1992. Application of time-
791 domain reflectometry (TDR) soil moisture miniprobe for the determination of
792 unsaturated soil water characteristics from undisturbed soil cores. Irrig. Sci. 13(2): 65-
793 72. doi:10.1007/BF00193982

794 Mangel, A.R., Moysey, S.M.J., Ryan, J.C., Tarbutton, J.A., 2012. Multi-offset ground-
795 penetrating radar imaging of a lab-scale infiltration test. Hydrol. Earth Syst. Sci.
796 16(11): 4009-4022. doi:10.5194/hess-16-4009-2012

797 Mangel, A.R., Moysey, S.M.J., van der Kruk, J., 2017. Resolving infiltration-induced
798 water content profiles by inversion of dispersive ground-penetrating radar data.
799 Vadose Zone J. 16(10): vzj2017.02.0037. doi:10.2136/vzj2017.02.0037

800 Manoli, G., Rossi, M., Pasetto, D., Deiana, R., Ferraris, S., Cassiani, G., Putti, M., 2015.
801 An iterative particle filter approach for coupled hydro-geophysical inversion of a
802 controlled infiltration experiment. J. Comput. Phys. 283: 37-51.
803 doi:10.1016/j.jcp.2014.11.035

804 Martínez-Vilalta, J., Piñol, J., Beven, K., 2002. A hydraulic model to predict drought-
805 induced mortality in woody plants: an application to climate change in the
806 Mediterranean. Ecol. Modell. 155(2): 127-147. doi:10.1016/S0304-3800(02)00025-X

807 Mboh, C.M., Huisman, J.A., Van Gaelen, N., Rings, J., Vereecken, H., 2012. Coupled
808 hydrogeophysical inversion of electrical resistances and inflow measurements for
809 topsoil hydraulic properties under constant head infiltration. Near Surf. Geophys. 10(5):
810 413-426. doi:10.3997/1873-0604.2012009

811 Mboh, C.M., Huisman, J.A., Vereecken, H., 2011. Feasibility of sequential and coupled
812 inversion of time domain reflectometry data to infer soil hydraulic parameters under
813 falling head infiltration. Soil Sci. Soc. Am. J. 75(3): 775-786.
814 doi:10.2136/sssaj2010.0285

815 McDowell, N.G., Allen, C.D., 2015. Darcy's law predicts widespread forest mortality

under climate warming. Nat. Clim. Chang. 5(7): 669-672. doi:10.1038/nclimate2641

Moghadas, D., Jadoon, K.Z., McCabe, M.F., 2017. Spatiotemporal monitoring of soil water content profiles in an irrigated field using probabilistic inversion of time-lapse EMI data. Adv. Water Resour. 110: 238-248. doi:https://doi.org/10.1016/j.advwatres.2017.10.019

Moysey, S.M., 2010. Hydrologic trajectories in transient ground-penetrating-radar reflection data. GEOPHYSICS. 75(4): WA211-WA219. doi:10.1190/1.3463416

Mualem, Y., 1976. A new model for predicting the hydraulic conductivity of unsaturated porous media. Water Resour. Res. 12(3): 513-522. doi:10.1029/WR012i003p00513

Nandagiri, L., Prasad, R., 1996. Field evaluation of unsaturated hydraulic conductivity models and parameter estimation from retention data. J. Hydrol. 179(1): 197-205. doi:10.1016/0022-1694(95)02840-4

Neuzil, C.E., Cooley, C., Silliman, S.E., Bredehoeft, J.D., Hsieh, P.A., 1981. A transient laboratory method for determining the hydraulic properties of 'tight' rocks—II. Application, International Journal of Rock Mechanics and Mining Sciences & Geomechanics Abstracts, pp. 253-258. doi:10.1016/0148-9062(81)90980-3

Pollock, D., Cirpka, O.A., 2010. Fully coupled hydrogeophysical inversion of synthetic salt tracer experiments. Water Resour. Res. 46(7). doi:10.1029/2009wr008575

Redman, D., Parkin, G.W., Annan, A.P., 2000. Borehole GPR measurement of soil water content during an infiltration experiment, Eighth International Conference on

837 Ground Penetrating Radar. International Society for Optics and Photonics, pp. 501-505.

838 Robinson, D.A., Jones, S.B., Blonquist, J.M., Friedman, S.P., 2005. A Physically
839 Derived Water Content/Permittivity Calibration Model for Coarse-Textured, Layered
840 Soils. Soil Sci. Soc. Am. J. 69(5): 1372-1378. doi:10.2136/sssaj2004.0366

841 Robinson, D.A., Campbell, C.S., Hopmans, J.W., Hornbuckle, B.K., Jones, S.B., Knight,
842 R., Ogden, F., Selker, J., Wendroth, O., 2008. Soil Moisture Measurement for
843 Ecological and Hydrological Watershed-Scale Observatories: A Review. Vadose Zone
844 J. 7(1): 358-389. doi:10.2136/vzj2007.0143

845 Rossi, M., Manoli, G., Pasetto, D., Deiana, R., Ferraris, S., Strobbia, C., Putti, M.,
846 Cassiani, G., 2015. Coupled inverse modeling of a controlled irrigation experiment
847 using multiple hydro-geophysical data. Adv. Water Resour. 82: 150-165.
848 doi:10.1016/j.advwatres.2015.03.008

849 Roth, K., Schulin, R., Flühler, H., Attinger, W., 1990. Calibration of time domain
850 reflectometry for water content measurement using a composite dielectric approach.
851 Water Resour. Res. 26(10): 2267-2273. doi:10.1029/WR026i010p02267

852 Rovey, C.W., II and Cherkauer, D.S., 1995. Scale dependency of hydraulic conductivity
853 measurements. Groundwater. 33(5): 769-780. doi:10.1111/j.1745-
854 6584.1995.tb00023.x

855 Rucker, D.F., Ferré, T.P.A., 2004a. Correcting water content measurement errors
856 associated with critically refracted first arrivals on zero offset profiling borehole
857 ground penetrating radar profiles. Vadose Zone J. 3(1): 278-287.
858 doi:10.2136/vzj2004.2780

859 Rucker, D.F., Ferré, T.P.A., 2004b. Parameter Estimation for Soil Hydraulic Properties
860 Using Zero-Offset Borehole Radar. Soil Sci. Soc. Am. J. 68(5): 1560-1567.
861 doi:10.2136/sssaj2004.1560

862 Schaap, M.G., Leij, F.J., 2000. Improved prediction of unsaturated hydraulic
863 conductivity with the Mualem - van Genuchten model. Soil Sci. Soc. Am. J. 64(3):
864 843-851. doi:10.2136/sssaj2000.643843x

865 Šimůnek, J., van Genuchten, M.T., Šejna, M., 2008. Development and applications of
866 the HYDRUS and STANMOD software packages and related codes. Vadose Zone J.
867 7(2): 587-600. doi:10.2136/vzj2007.0077

868 Slob, E., Sato, M., Olhoeft, G., 2010. Surface and borehole ground-penetrating-radar
869 developments. GEOPHYSICS. 75(5): 75A103-75A120. doi:10.1190/1.3480619

870 Steelman, C.M., Endres, A.L., Jones, J.P., 2012. High-resolution ground-penetrating
871 radar monitoring of soil moisture dynamics: Field results, interpretation, and
872 comparison with unsaturated flow model. Water Resour. Res. 48(9).
873 doi:10.1029/2011wr011414

874 Steenpass, C., Vanderborght, J., Herbst, M., Šimůnek, J., Vereecken, H., 2010.
875 Estimating soil hydraulic properties from infrared measurements of soil surface
876 temperatures and TDR data. Vadose Zone J. 9(4): 910-924. doi:10.2136/vzj2009.0176

877 Thyer, M., Kuczera, G., Bates, B.C., 1999. Probabilistic optimization for conceptual
878 rainfall-runoff models: A comparison of the shuffled complex evolution and simulated
879 annealing algorithms. Water Resour. Res. 35(3): 767-773. doi:10.1029/1998wr900058

880 Toorman, A.F., Wierenga, P.J., Hills, R.G., 1992. Parameter estimation of hydraulic
881 properties from one-step outflow data. Water Resour. Res. 28(11): 3021-3028.
882 doi:10.1029/92wr01272

883 Topp, G.C., Davis, J.L., Annan, A.P., 1980. Electromagnetic determination of soil water
884 content: Measurements in coaxial transmission lines. Water Resour. Res. 16(3): 574-
885 582. doi:10.1029/WR016i003p00574

886 van Genuchten, M.T., 1980. A Closed-form Equation for Predicting the Hydraulic
887 Conductivity of Unsaturated Soils. Soil Sci. Soc. Am. J. 44(5): 892-898.
888 doi:10.2136/sssaj1980.03615995004400050002x

889 van Overmeeren, R.A., Sariowan, S.V., Gehrels, J.C., 1997. Ground penetrating radar
890 for determining volumetric soil water content; results of comparative measurements at
891 two test sites. J. Hydrol. 197(1): 316-338. doi:10.1016/S0022-1694(96)03244-1

892 Vereecken, H., Huisman, J.A., Bogena, H., Vanderborght, J., Vrugt, J.A., Hopmans,
893 J.W., 2008. On the value of soil moisture measurements in vadose zone hydrology: A
894 review. Water Resour. Res. 44(4). doi:10.1029/2008wr006829

895 Vereecken, H., Kasteel, R., Vanderborght, J., Harter, T., 2007. Upscaling hydraulic
896 properties and soil water flow processes in heterogeneous soils: A Review. Vadose
897 Zone J. 6(1): 1-28. doi:10.2136/vzj2006.0055

898 Vrugt, J., Dane, J., 2006. Inverse Modeling of Soil Hydraulic Properties, In
899 Encyclopedia of Hydrological Sciences. doi:10.1002/0470848944.hsa079

900 Wagner, B.J., 1992. Simultaneous parameter estimation and contaminant source

characterization for coupled groundwater flow and contaminant transport modelling. J. Hydrol. 135(1): 275-303. doi:10.1016/0022-1694(92)90092-A

Warren, C., Giannopoulos, A., Giannakis, I., 2016. gprMax: Open source software to simulate electromagnetic wave propagation for Ground Penetrating Radar. Comput. Phys. Commun. 209: 163-170. doi:10.1016/j.cpc.2016.08.020

Weihermüller, L., Huisman, J.A., Lambot, S., Herbst, M., Vereecken, H., 2007. Mapping the spatial variation of soil water content at the field scale with different ground penetrating radar techniques. J. Hydrol. 340(3): 205-216. doi:10.1016/j.jhydrol.2007.04.013

Wollschläger, U., Pfaff, T., Roth, K., 2009. Field-scale apparent hydraulic parameterisation obtained from TDR time series and inverse modelling. Hydrol. Earth Syst. Sci. 13(10): 1953-1966. doi:10.5194/hess-13-1953-2009

Yu, Y., Klotzsche, A., Weihermüller, L., Huisman, J.A., Vanderborght, J., Vereecken, H., van der Kruk, J., 2020. Measuring vertical soil water content profiles by combining horizontal borehole and dispersive surface ground penetrating radar data. Near Surf. Geophys. 18(3): 275-294. doi:10.1002/nsg.12099

Zhang, Z.F., Ward, A.L., Gee, G.W., 2003. Estimating soil hydraulic parameters of a field drainage experiment using inverse techniques. Vadose Zone J. 2(2): 201-211. doi:10.2136/vzj2003.2010

Zhu, J., Mohanty, B.P., 2003. Effective hydraulic parameters for steady state vertical flow in heterogeneous soils. Water Resour. Res. 39(8). doi:10.1029/2002wr001831

Table 1

Soil texture of fine soil, mass fraction of stones and porosity of the field according to Cai et al. (2016)

Depth	Sand	Silt	Clay	Stones	Porosity
cm	——————Vol % ——————			Mass %	
Topsoil (0 - 30)	35	52	13	50	0.33
Subsoil (30 – 120)	37	47	16	69	0.25

Table 2

Soil hydraulic parameters according to Cai et al. (2017) for the rhizotron facility.

Depth	θ_r	θ_s	α	n	K_s	l
cm	cm^3cm^{-3}		cm^{-1}	-	cm min^{-1}	-
0 - 30	0.043	0.326	0.036	1.386	0.057	1.47
30- 120	0.053	0.229	0.050	1.534	0.0004†;0.04††	-2.78

† The K_s value of subsoil estimated by Cai et al. (2017).
†† The K_s value used for synthetic study of 2-layered soil profile.

Table 3

Inverted results of noisy synthetic data

	True value	Bounds	Inverted results	
			Sequential inversion	Coupled inversion
		homogenous soil profile		
θ_s (cm^3cm^{-3})	0.326	0.25 – 0.40	0.290	0.326±0.001†
α (cm^{-1})	0.036	0.030 – 0.125	0.106	0.036±0.003
n	1.386	1.1 – 2.8	1.431	1.358±0.016
$\log(K_s)$ (cm min^{-1})	-1.244	-1.456 – -0.276	-1.456	-1.168±0.038
Cost-function	-	-	0.05	0.1
		2-layered soil profile		
θ_{s1} (cm^3cm^{-3})	0.326	0.30 – 0.40	0.345	0.324±0.007
α_1 (cm^{-1})	0.036	0.030 – 0.125	0.036	0.036±0.004
n_1	1.386	1.1 – 2.8	1.506	1.312±0.024
$\log(K_{s1})$ (cm min^{-1})	-1.244	-1.456 – -0.276	-0.276	-0.996±0.048
θ_{s2} (cm^3cm^{-3})	0.229	0.15 – 0.30	0.300	0.240±0.007
α_2 (cm^{-1})	0.050	0.030 – 0.125	0.038	0.045±0.004
n_2	1.534	1.1 – 2.8	1.696	1.431±0.020
$\log(K_{s2})$ (cm min^{-1})	-1.398	-1.456 – -0.276	-1.456	-1.108±0.048
Cost-function	-	-	0.01	0.1

†The values indicated the 99% confidence interval based on the first-order approximation.

Table 4

Correlation matrix of the estimated hydraulic parameters for the homogeneous profile

	α (cm^{-1})	n (-)	$\log(K_s)$ ($min\ cm^{-1}$)	θ_s (cm^3cm^{-3})
n	-0.335	1		
$\log(K_s)$	0.233	-0.694†	1	
θ_s	-0.086	0.256	0.186	1

†The values indicated the pairs of parameters showing strong correlation.

Table.5

Inverted Soil hydraulic parameters for the rhizotron facility from measured GPR data.

Depth	θ_r	θ_s	α	n	$\log(K_s)$	l
cm	cm^3cm^{-3}		cm^{-1}	-	cm min^{-1}	-
		[cost-function = 0.32 (ns)]				
0 – 30	0	0.328±0.011†	0.032±0.011	1.125±0.028	-0.983±0.266	0.5
30 - 120	0	0.196±0.009	0.038±0.015	1.202±0.054	-1.022±0.349	0.5

†The values indicated the 99% confidence interval based on the first-order approximation.

Table 6

Correlation matrix of the inverted hydraulic parameters for the 2-layered model

	α_1	n_1	$\log(K_{s1})$	α_2	n_2	$\log(K_{s2})$	θ_{s1}	θ_{s2}
	cm^{-1}	-	$min\ cm^{-1}$	cm^{-1}	-	$min\ cm^{-1}$	cm^3cm^{-3}	cm^3cm^{-3}
n_1	-0.388	1						
$\log(K_{s1})$	0.324	0.045	1					
α_2	-0.077	0.129	0.138	1				
n_2	-0.119	-0.139	-0.163	-0.069	1			
$\log(K_{s2})$	0.061	-0.059	-0.046	0.549	-0.615†	1		
θ_{s1}	-0.032	-0.226	0.189	0.040	-0.087	0.049	1	
θ_{s2}	-0.058	-0.347	-0.192	-0.083	0.404	0.070	-0.192	1

†The values indicated the pairs of parameters showing strong correlation.

Fig. 1. (a) Schedule and amount of irrigated water for the five infiltration events and (b) GPR travel time data measured at 6 different depths during the infiltration experiment. The timing of the infiltration events was indicated by light green background. The spatial variation of the travel times along the 5.5 m borehole tube is indicated by the error bars. Note that different y-axis scales are used for the results of different depths.

Fig. 2. Flow charts of (a) sequential inversion and (b) coupled inversion.

Fig. 3. (a) The source wavelet. (b) A synthetic trace of air wave generated by gprMax3D. (c) A synthetic vertical SWC profile generated by HYDRUS-1D. (d) Six synthetic GPR traces obtained using the synthetic vertical SWC distribution shown in (c). The red crosses indicate the first arrival time of the GPR traces.

Fig. 4. (a) Schedule of the synthetic infiltration events and synthetic GPR measurements. (b) Synthetic vertical SWC profiles from HYDRUS-1D (solid lines) and synthetic vertical SWC profiles estimated by GPR data (dashed lines) based on the vertical water content distribution used as inputs in gprMax3D. The colors indicate different measurement times. The GPR estimated SWCs at 0.2 – 1.2 m depth were inverted using a sequential inversion approach to estimate the hydraulic parameters for the 1-layer soil. (c) Differences between GPR-estimated and simulated HYDRUS-1D SWCs. The timing of the infiltration events is indicated by the light green background. Note that different y-axis scales are used for the results of different depths.

Fig. 5. Response surfaces for different pairs of hydraulic parameters obtained using (a) true SWC data simulated by HYDRUS-1D and (b) noise-free synthetic GPR travel times. The cost function values are shown in logarithmic scale. Blank spaces indicate that the hydrological model did not converge for the selected parameters. The global minimum of the cost function is shown by the red cross. Also note that the cost functions of sequential and coupled inversion ($C_{MVG}(\theta)$ and $C_{MVG}(t)$) have different units (cm^3cm^{-3} and ns, respectively).

Fig. 6. (a) Sequential inversion results of noisy GPR SWC estimations. (b) Coupled inversion results of noisy GPR travel time data. SWC data at 0.1 m depth was not used for sequential inversion. The timing of the infiltration events is indicated by the light green background. Note that different y-axis scales are used to show the results for different depths.

Fig. 7. Vertical SWC profiles of the (a) 1-layer and (b) 2-layer soil profile, which were simulated by using the true model (black solid line), parameters estimated from the coupled inversion (purple dashed line) and sequential inversion (yellow dashed line) at four different measurement times. Note that the different background indicates the different layers.

Fig. 8. Water retention $\theta(h)$ and relative hydraulic conductivity $K_r(h)$ function for the (a,b) synthetic homogeneous soil profile, and the (c,d) topsoil and (e,f) subsoil of the 2-layer profile.

Fig. 9. Coupled inversion results of noisy GPR travel time data for 2-layer profile. The timing of the infiltration events is indicated by the light green background. Please note that results for different depths are shown with difference range of y-axis scale.

Fig. 10. Coupled inversion results of measured GPR travel time data at different depths. Simulated travel time using the hydraulic parameters of Cai et al. (2017) and inverted model are shown in blue and black dashed lines, respectively. The timing of infiltration events is indicated by the light green background. Please note that different y-axis scales are used for the results at different depths.

Fig. 11. Vertical SWC profiles simulated by using hydraulic parameters from the inversion of measured data (black lines) and Cai et al. (2017) (blue lines). Note that the different backgrounds indicate the different soil types.

Fig. 12. Linear regression between measured and GPR travel time data obtained using the inverted hydraulic parameters (black squares) and the hydraulic parameters of Cai et al. (2017) (blue crosses). The 1:1 line is indicated by the dashed red line.

Fig. 13. Water retention $\theta(h)$ and relative hydraulic conductivity $K_r(h)$ function from 100 possible inverted hydraulic parameter sets (dark lines), the hydraulic parameters of Cai et al. (2017) (blue line) and the hydraulic parameters with the best fit (red line) for the (a, c) top soil and (b, d) subsoil.

Figure

Click here to access/download;Figure;Fig1.tif

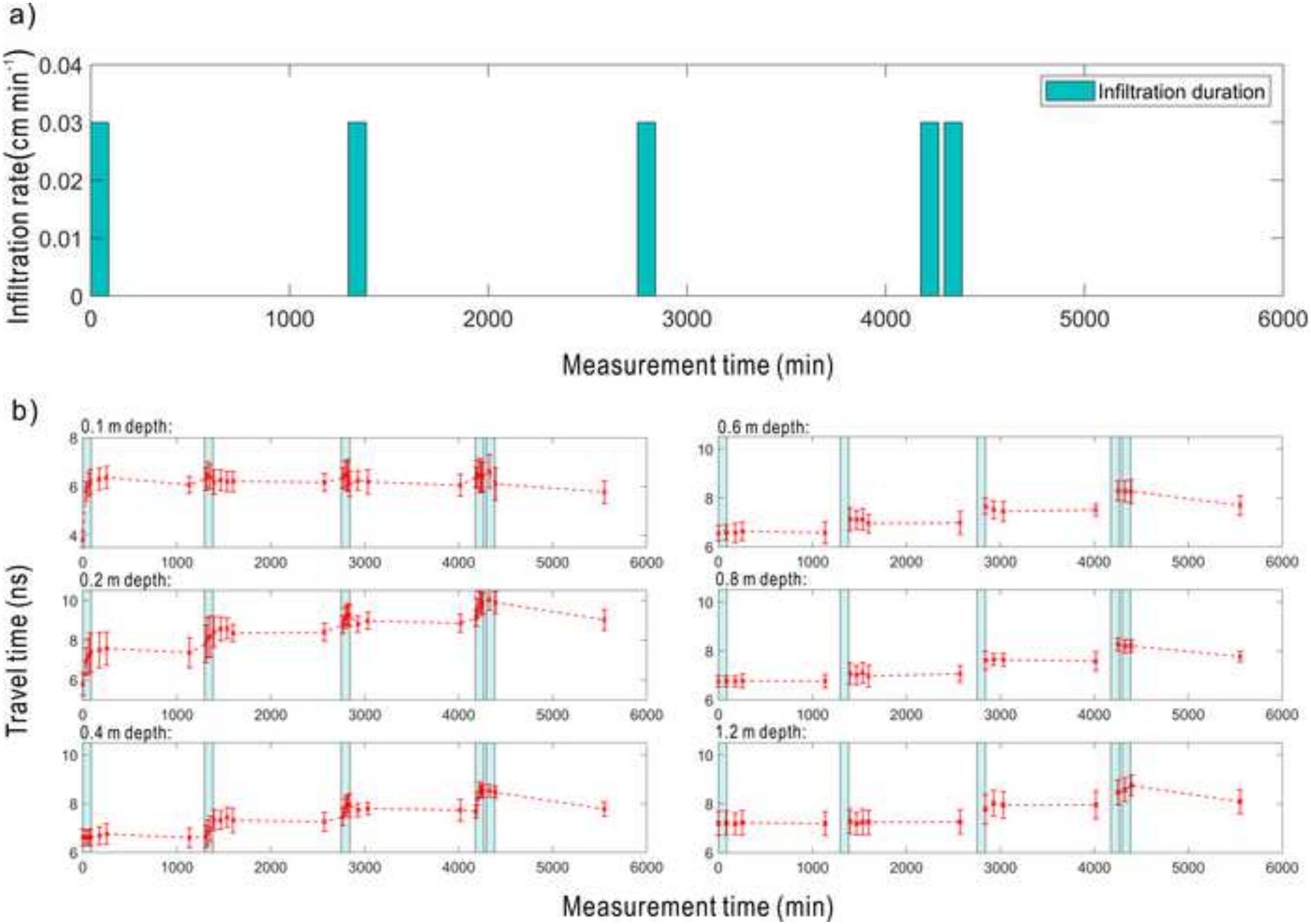

Figure

Click here to access/download;Figure;Fig2.tif

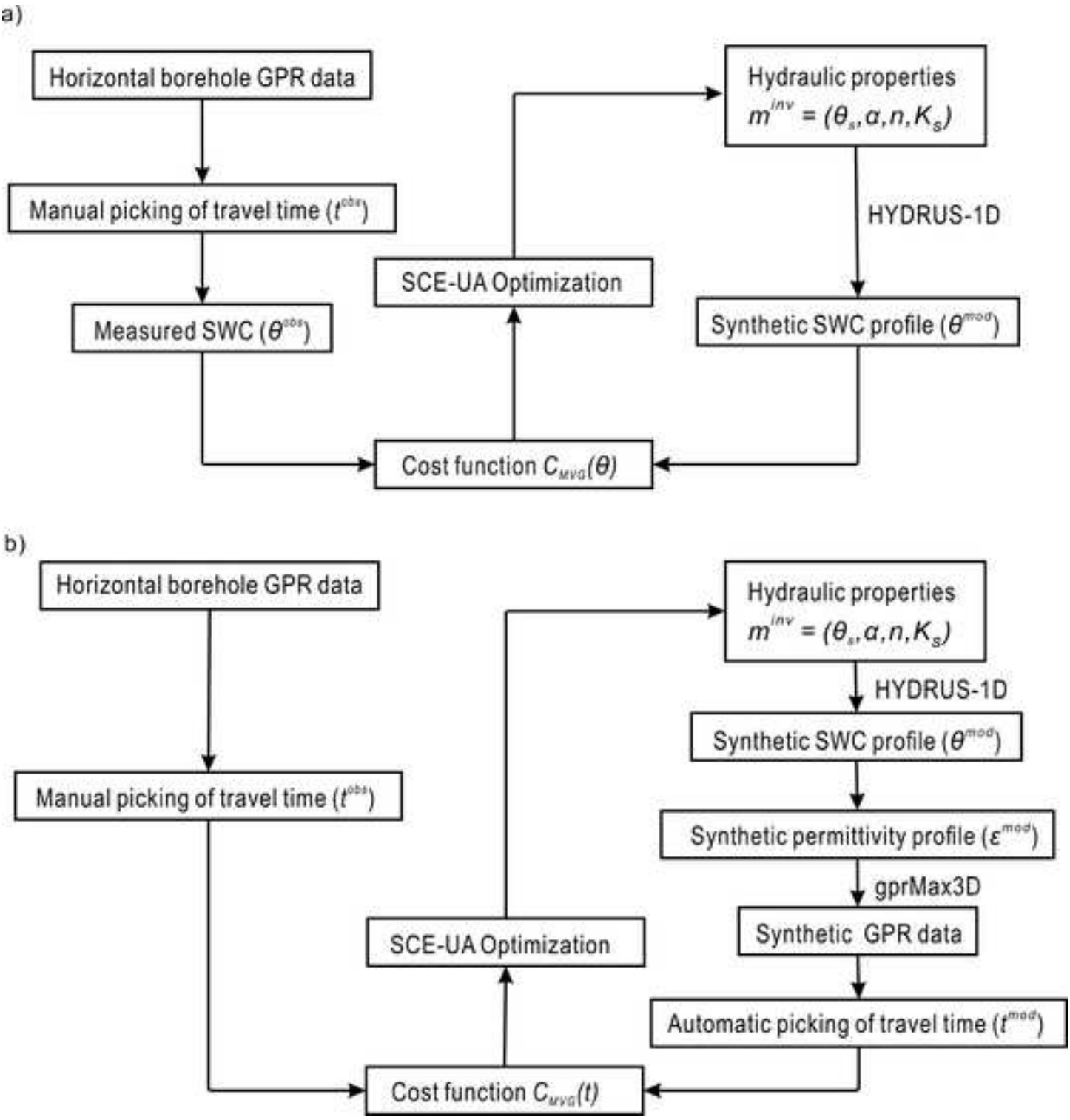

Figure

Click here to access/download;Figure;Fig3.tif

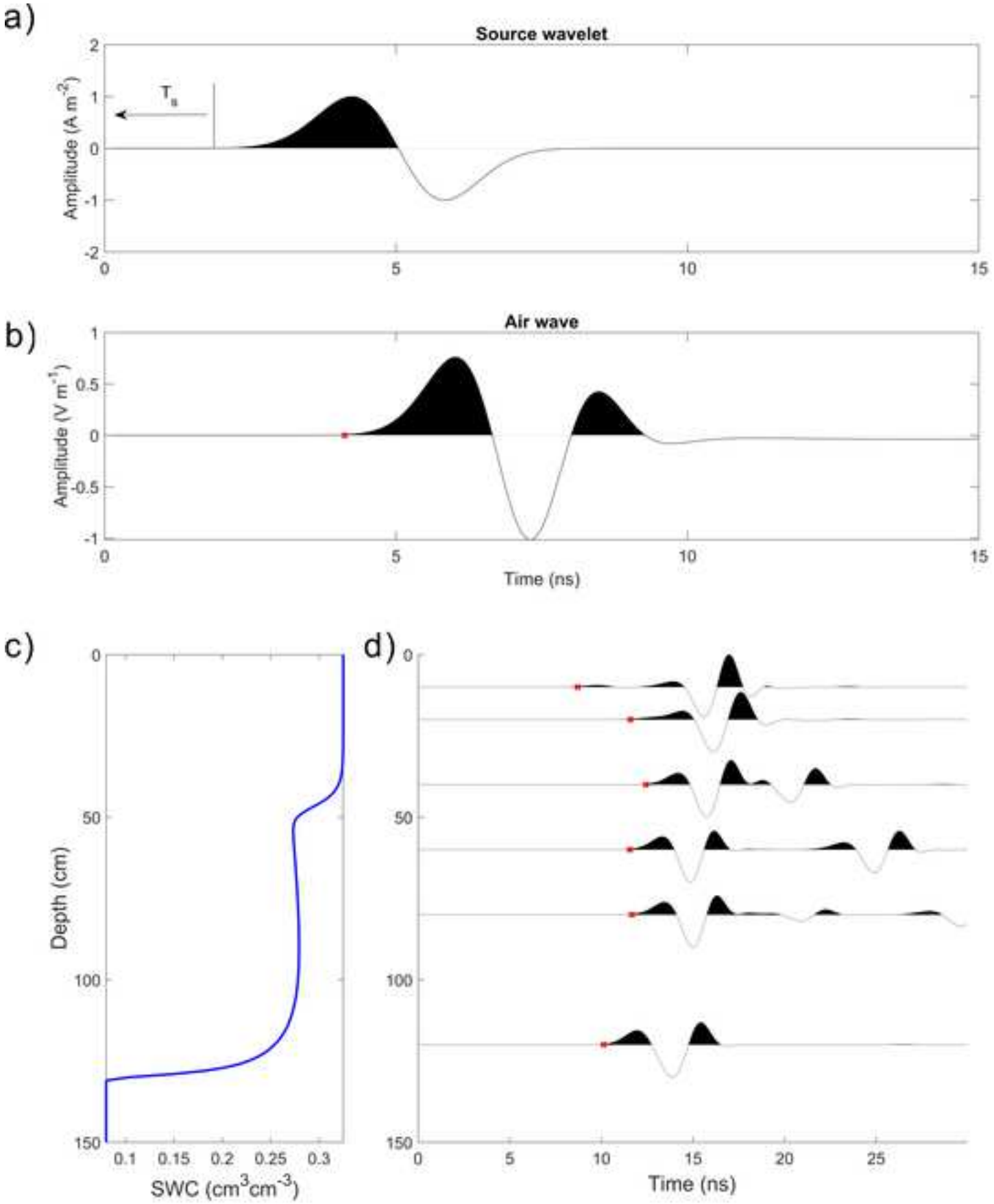

Figure

Click here to access/download;Figure;Fig4_Marked.tif

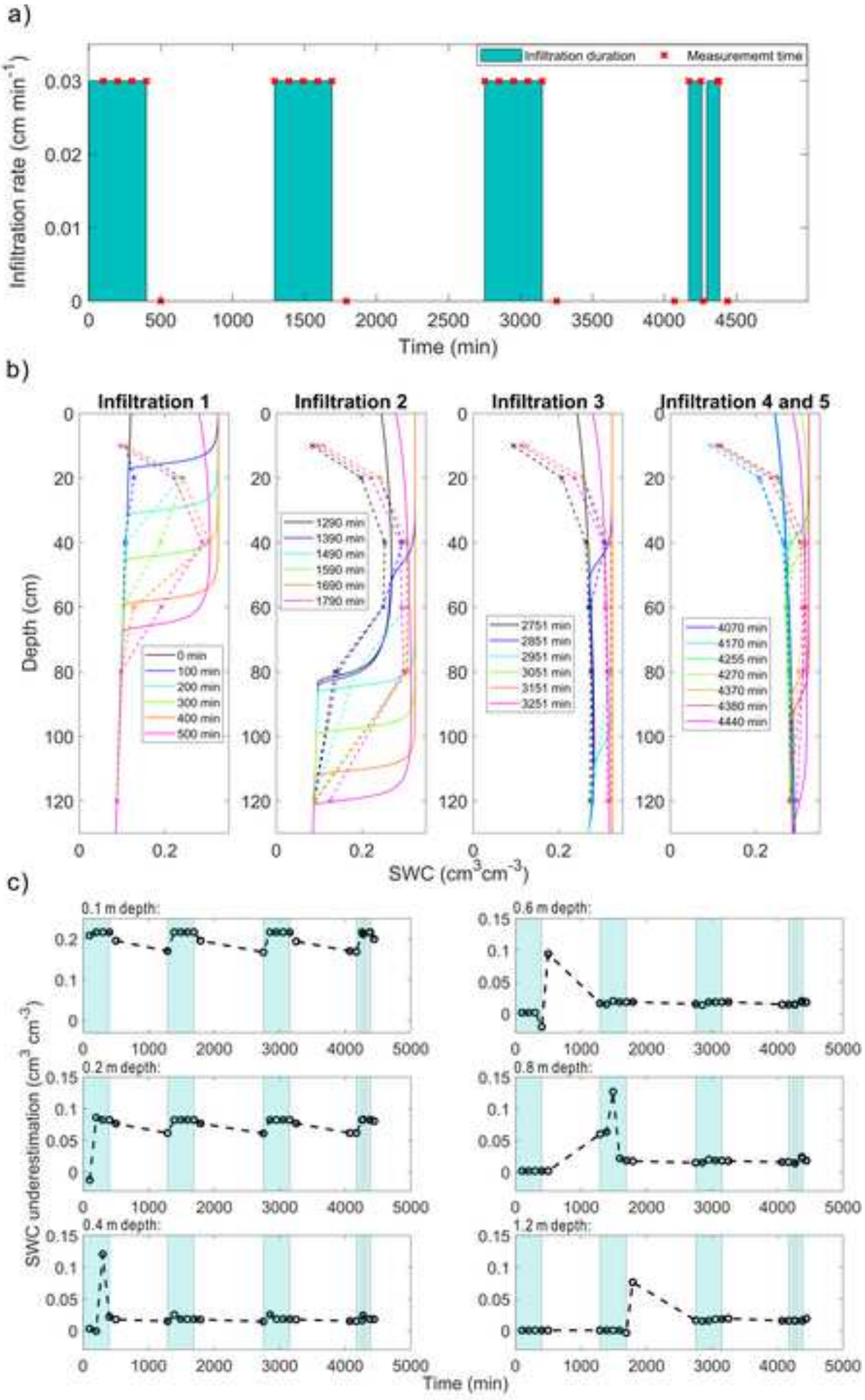

Figure

Click here to access/download;Figure;Fig5.tif

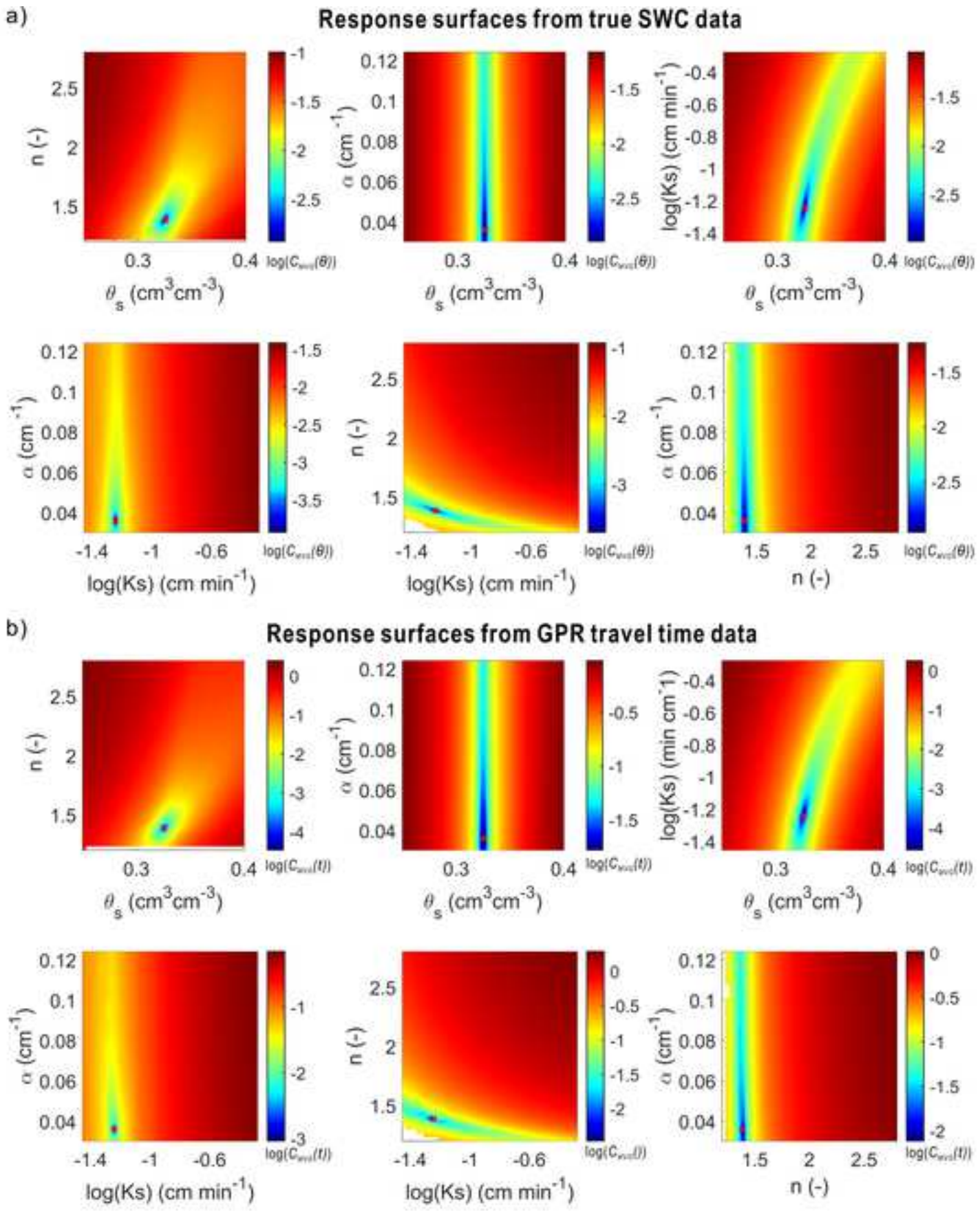

Figure

Click here to access/download;Figure;Fig6.tif

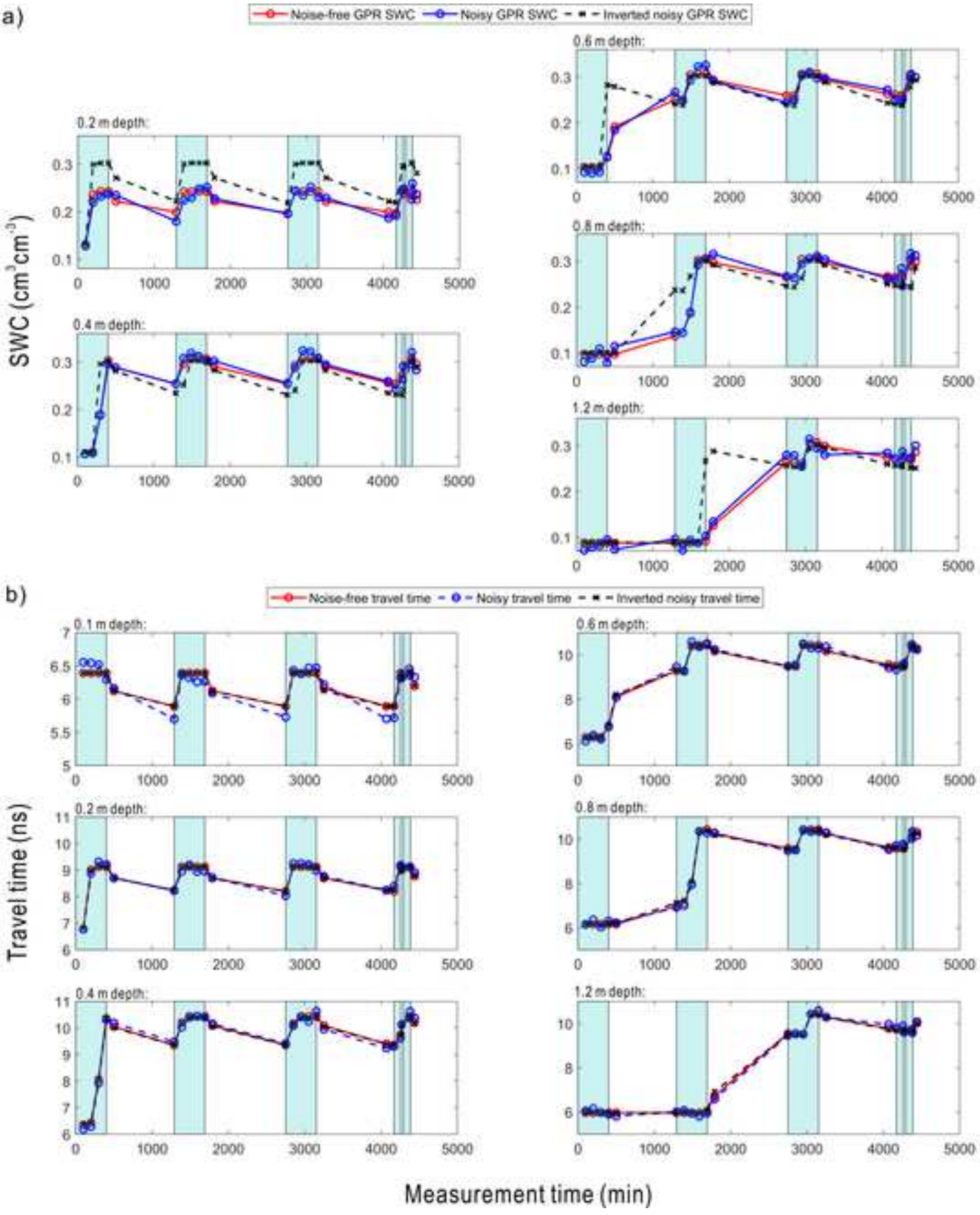

Figure

Click here to access/download;Figure;Fig7_Marked.tif

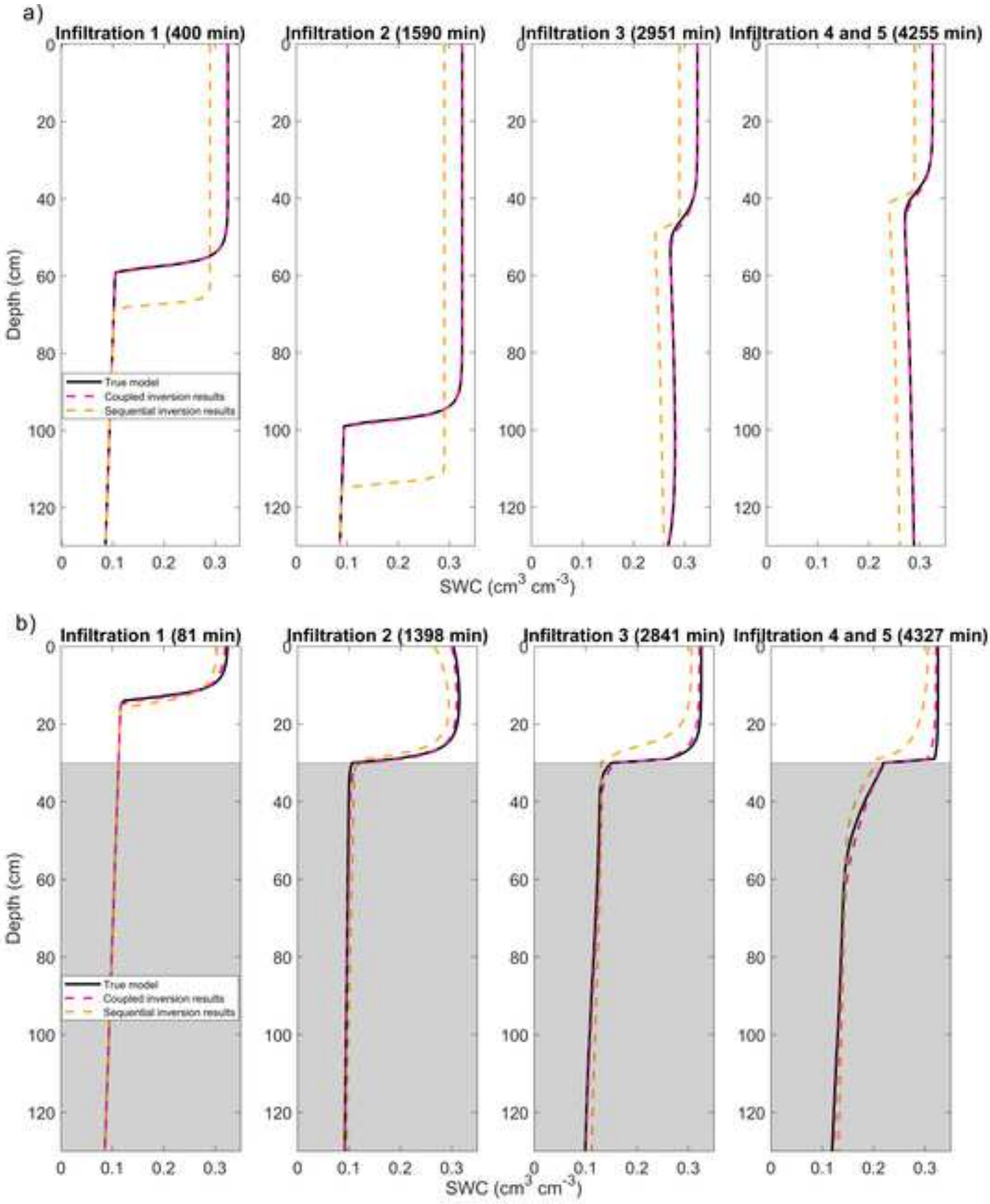

Figure

Click here to access/download;Figure;Fig8_Marked.tif

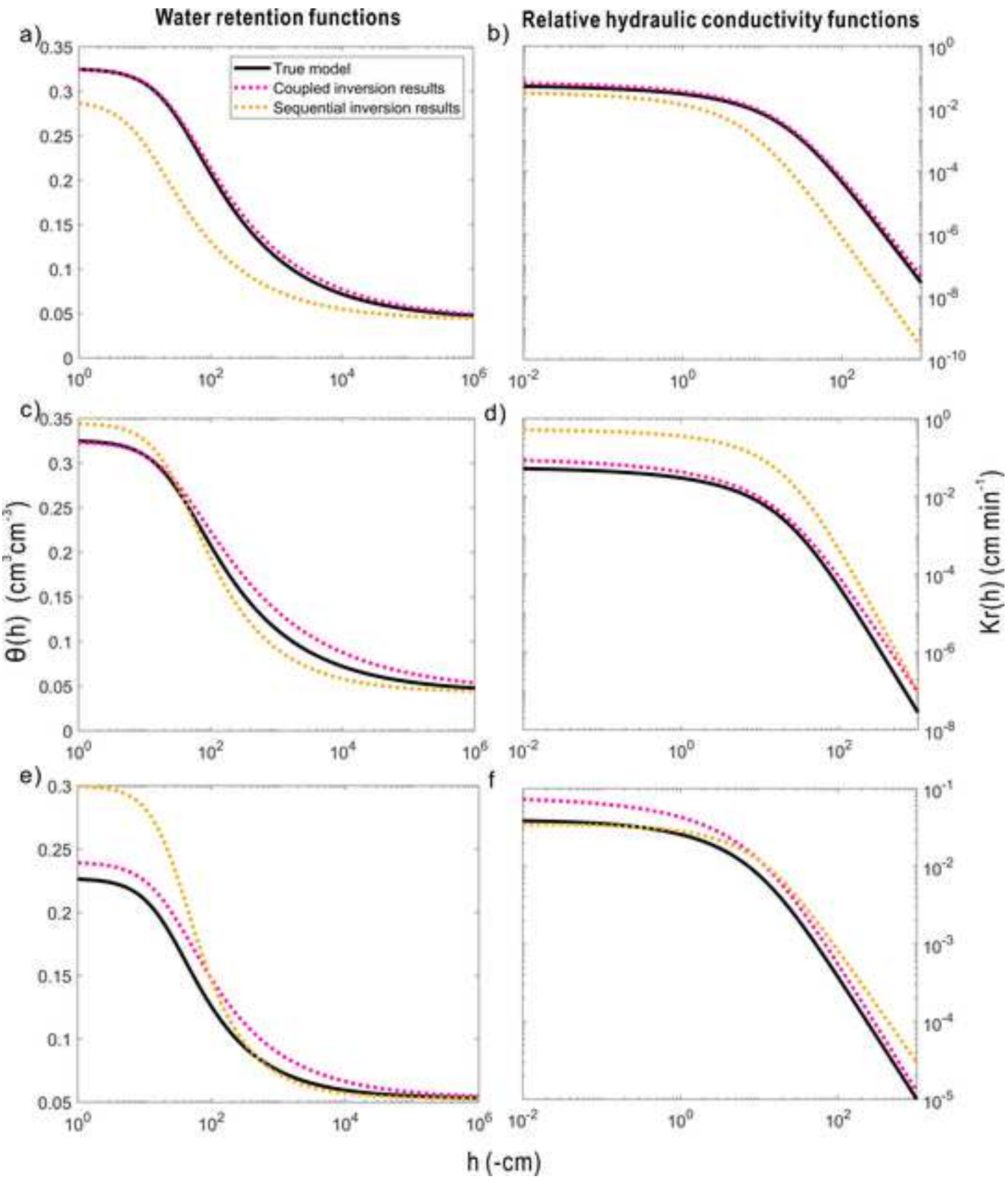

Figure

Click here to access/download;Figure;Fig9.tif

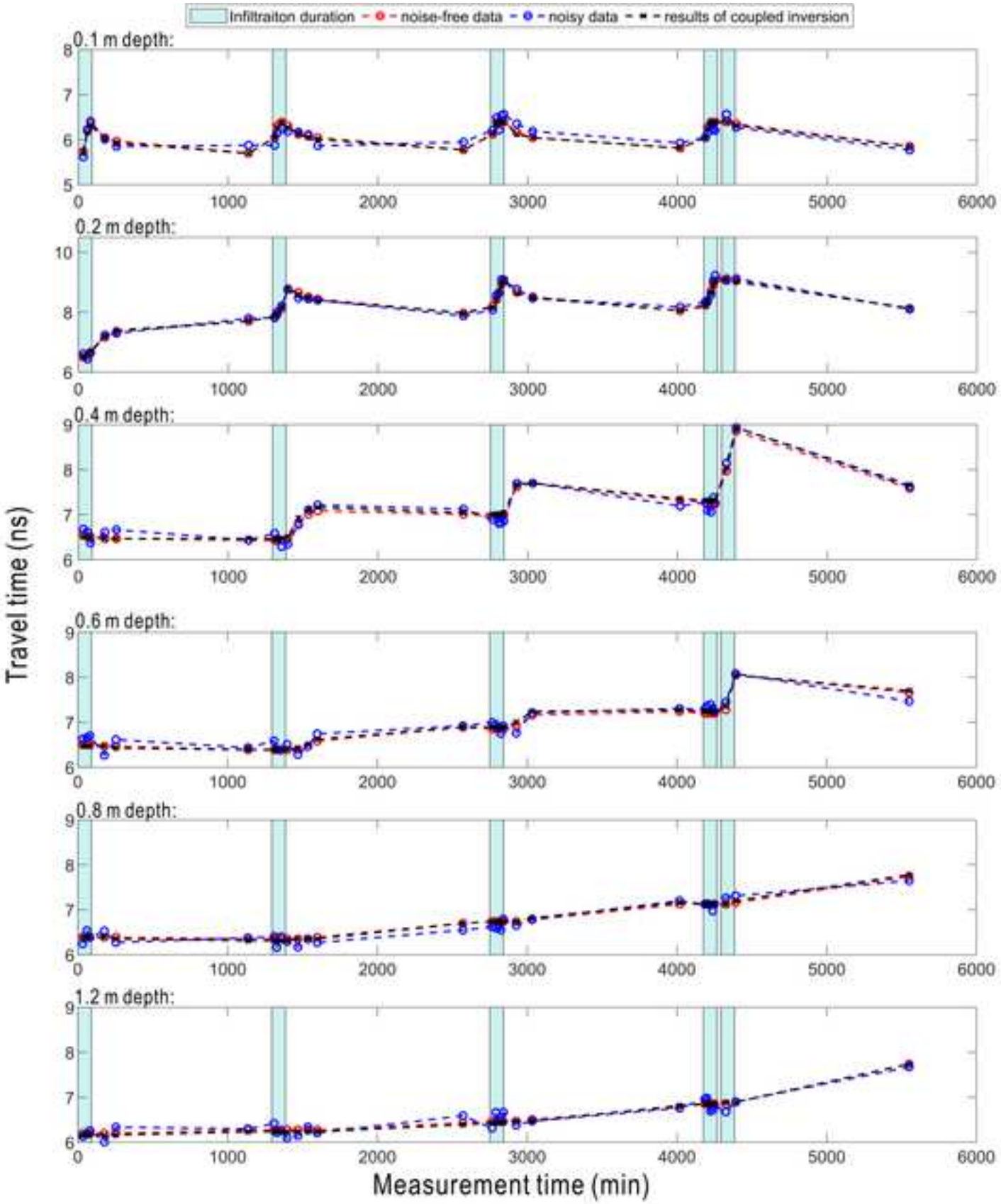

Figure

Click here to access/download;Figure;Fig10.tif

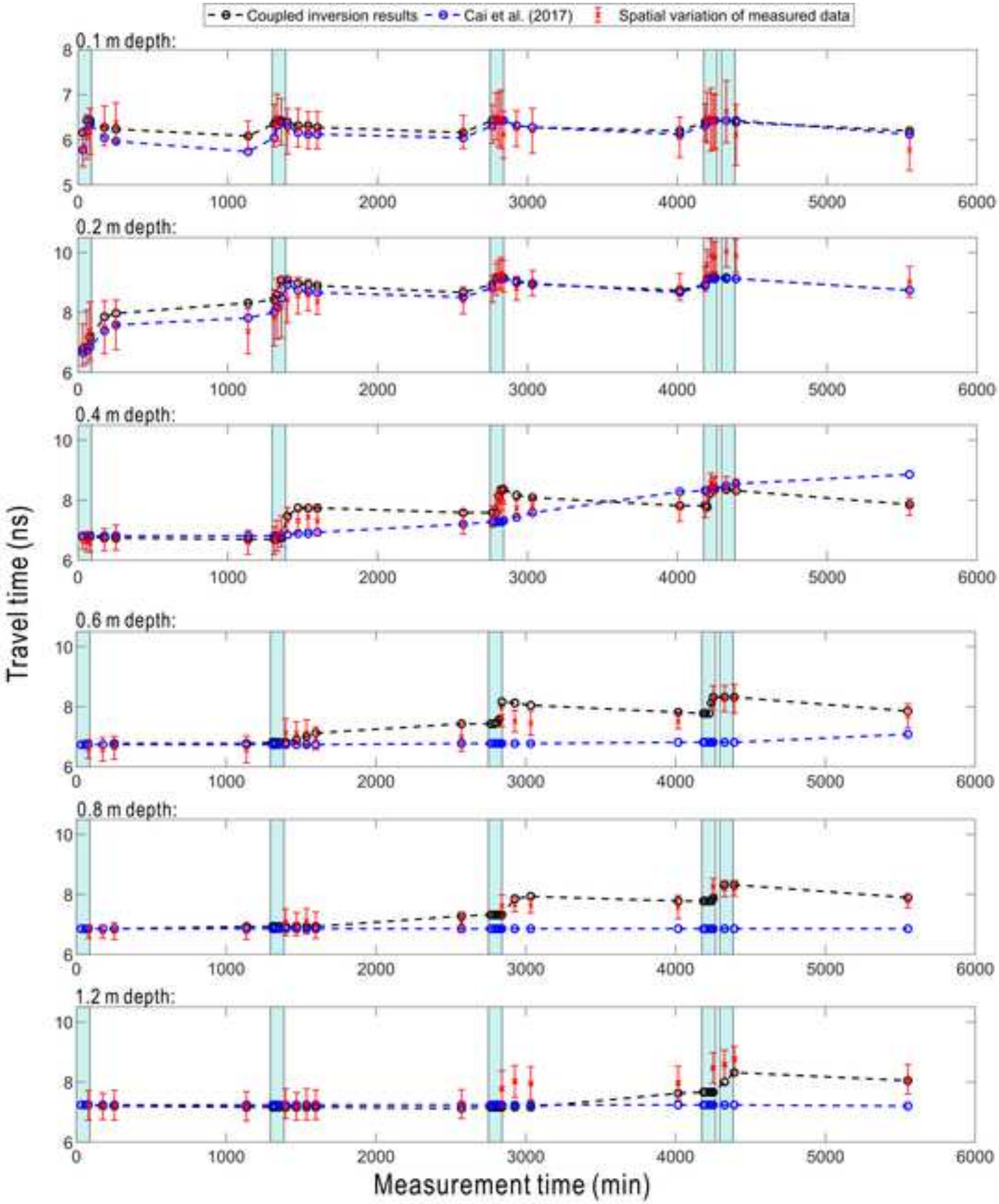

Figure

Click here to access/download;Figure;Fig11_Marked.tif

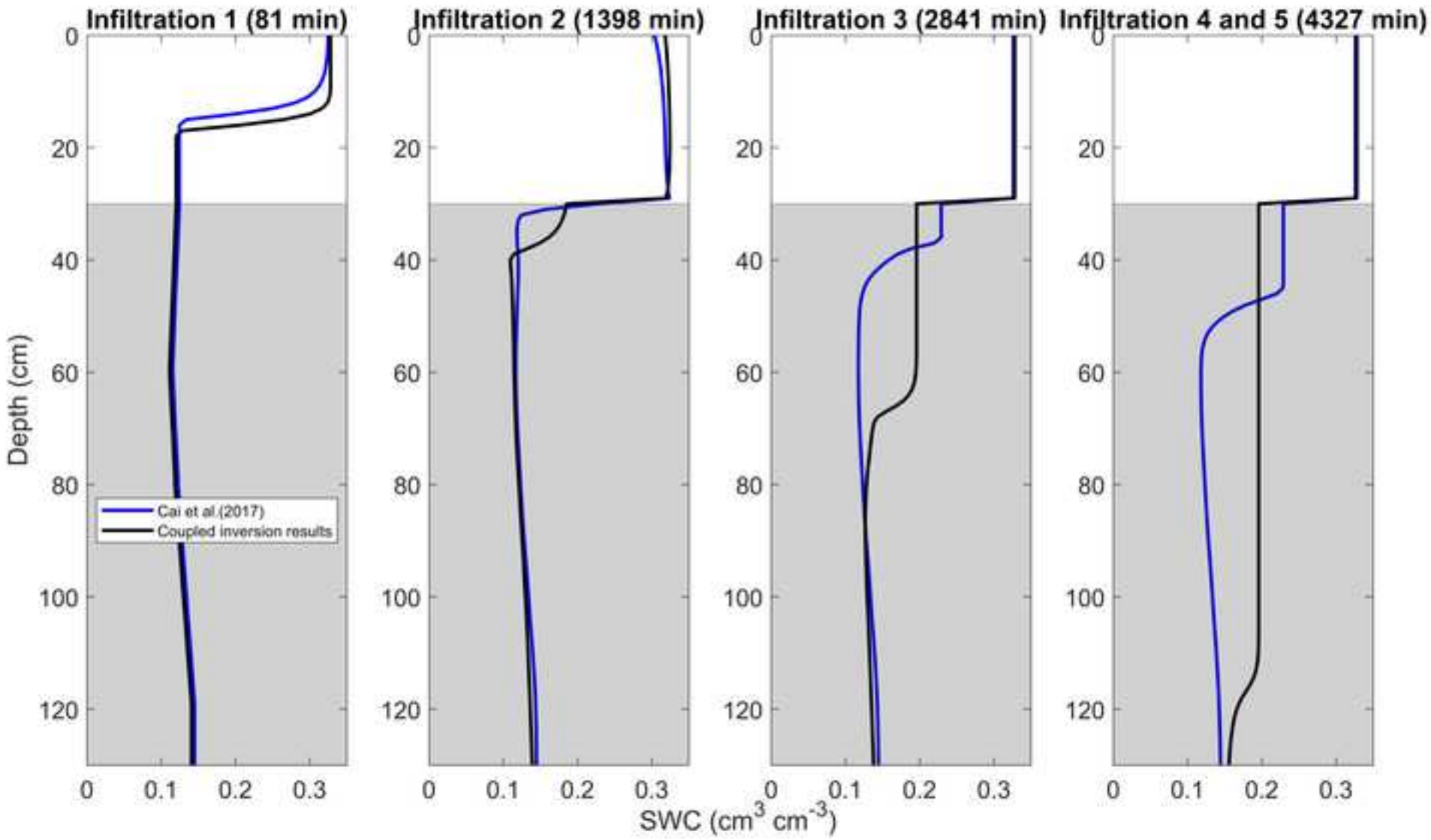

Figure

Click here to access/download;Figure;Fig12.tif

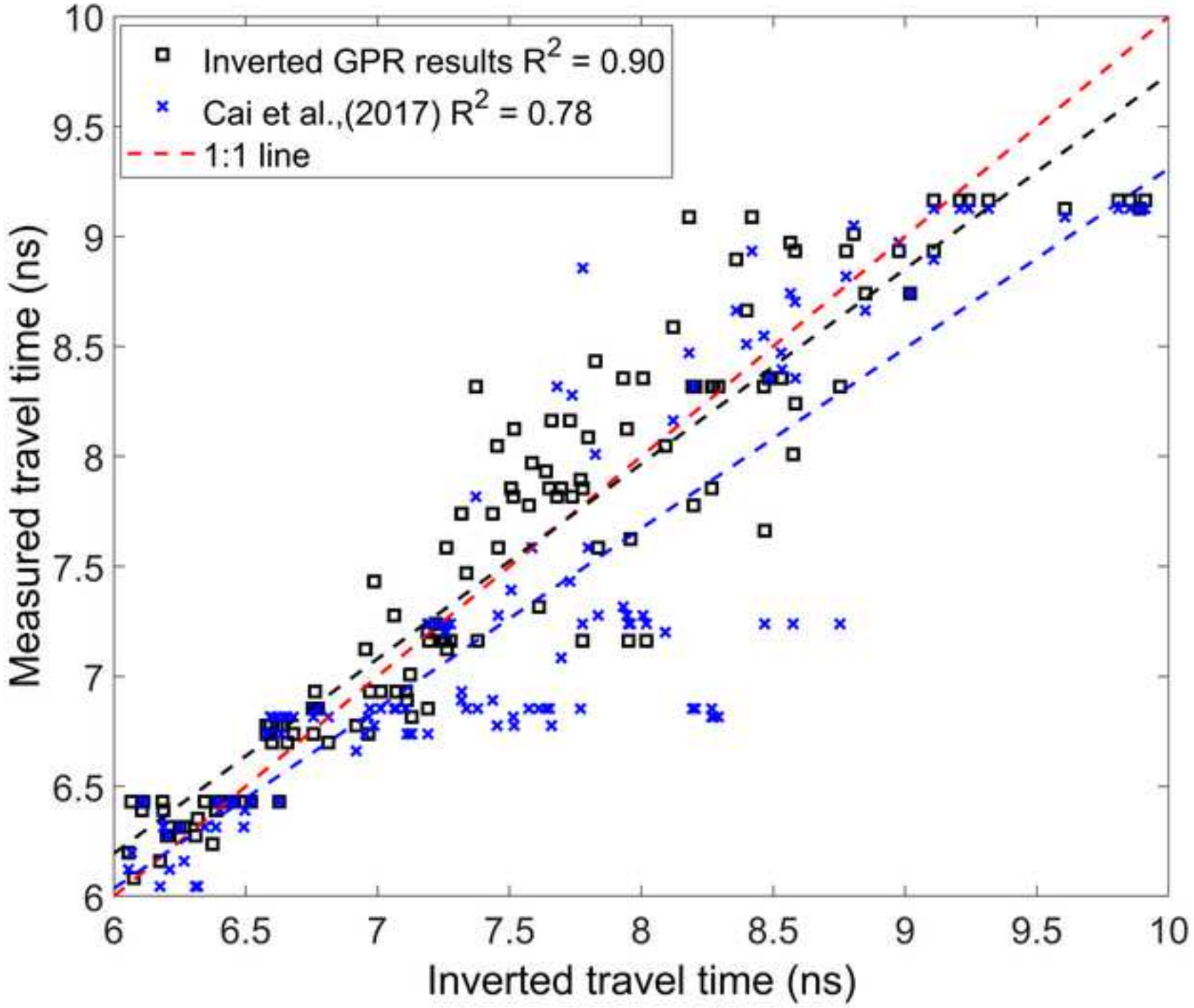

Figure

Click here to access/download;Figure;Fig13.tif

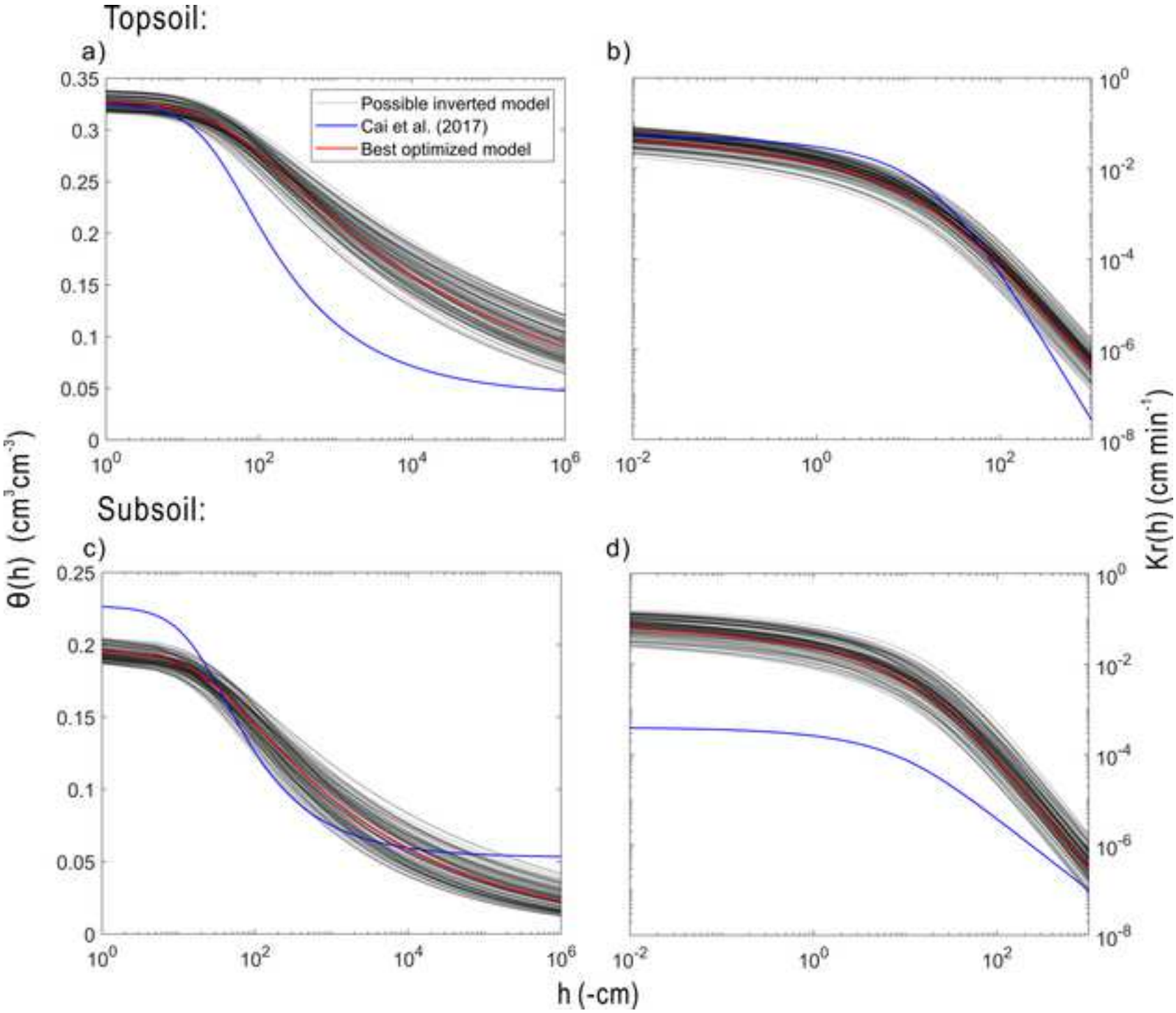

*Declaration of Interest Statement

Declaration of interests

☒ The authors declare that they have no known competing financial interests or personal relationships that could have appeared to influence the work reported in this paper.

☐The authors declare the following financial interests/personal relationships which may be considered as potential competing interests:

Yi Yu: Conceptualization; Methodology; Formal analysis; Writing - Original Draft.

Lutz Weihermüller: Conceptualization; Methodology; Writing - Review & Editing.

Anja Klotzsche: Methodology;Investigation; Resources.

Lena Lärm: Methodology; Software.

Harry Vereecken: Supervision; Project administration; Funding acquisition.

Johan Alexander Huisman: Conceptualization; Methodology; Writing - Review & Editing.